Title	Development of High-accurate Adsorption Instrument and Investigation on Surface Property and Porous Structure Using Adsorption Technique
Author(s)	其田，穣次
Citation	大阪大学，2010，博士論文
Version Type	VoR
URL	https://hdl.handle.net/11094/258
rights	
Note	

Development of High-accurate Adsorption Instrument and Investigation on Surface Property and Porous Structure Using Adsorption Technique

(高精度吸着装置の開発および吸着技術を用いた材料表面特性と細孔構造の研究)

Joji SONODA

其田　穣次

2009

Development of High-accurate Adsorption Instrument and Investigation on Surface Property and Porous Structure Using Adsorption Technique

(高精度吸着装置の開発および吸着技術を用いた材料表面特性と細孔構造の研究)

Joji SONODA

其田　穣次

2009

Contents

Chapter 1 General Introduction

Chapter 2 High Precision Volumetric Gas Adsorption Apparatus

Chapter 3 Adsorption Isotherm Measurement of N_2 from Extremely Low Relative Pressure (p/p_0=10^{-9}~) to Non-Porous and Microporous Carbon Materials

Chapter 4 High Resolution Argon Adsorption Isotherms for Various Zeolites

Chapter 5 High Resolution Adsorption Isotherm of N_2 and Ar for Nonporous Silicas and MFI Zeolites

Chapter 6 Hydrophobic Modification of Ti-containing Zeolite (TS-1) and Their Applications in the Liquid-phase Selective Catalytic Reaction

Chapter 1

General Introduction

1.1 Introduction

Recently, a variety of porous materials have been developed and they play important roles in the industrial fields.

Among them, zeolite is a typical crystalline microporous material. Although zeolites have been known for over 200 years, their potential for highly selective adsorbents was first realized about 50 years ago [1,2]. Since Breck et al. reported the synthetic method of the hitherto unknown zeolite A [3], several hundred zeolites have been synthesized. The synthesis of zeolites with the characteristic pore structure by designing their pore size and shape is an important issue.

Because of their molecular-level pore, zeolites have been used for adsorbents, gas separation, purification, ion-exchange and other applications. Recently, it is expected that zeolites can be used for new fields such as separation membrane, sensor and the laser element. However, the most important application of zeolites might be catalysts. Because of the high-selectivity and the large specific surface area, zeolites can be used not only for catalysts but also for catalyst supports. The ability of zeolites incorporated with heteroatoms such as Ti into the siliceous framework has been investigated. Needless to say, for such applications, the study on porous structure is very important [4,5].

To evaluate the surface area and the pore size distribution of porous materials, gas adsorption technique is widely used. In general, such properties can be calculated from the adsorption isotherm of inert gas at its boiling temperature (e.g. nitrogen at 77K, argon at 87K). As the recent progress of the porous material, various new methods for the interpretation of adsorption data have been introduced. Microporous material gives Type I isotherm, in which adsorption amount increases at low relative pressure range. It is very important to measure accurate adsorption isotherm in the relative pressure range to obtain the micropore size distribution.

1.2 Purpose of this study

Previously, one of the experimental apparatuses to achieve the measurements from low relative pressure as low as $p/p_0=10^{-9}$, was developed by Kaneko et al. [6], using a gravimetric technique. In general, gravimetric method has potential sources of error as follows [7].

- The buoyancy correction is necessary.
- Because of the poor thermal transport between the sample and the surrounding thermostat, it is difficult to obtain the thermal equilibrium.
- Sample bucket often sticks to the inner wall of the system as when it is electrostatically charged.

In the present study, at first, a new volumetric adsorption measuring system, BELSORP-max which can obtain accurate low pressure adsorption isotherms was developed. On developing the system, a new method to evaluate the dead volume was introduced. This method improved the accuracy and reproducibility of the adsorption isotherm measurement dramatically.

Using BELSORP-max, the measurements of nitrogen and argon adsorption isotherms were carried out for two nonporous silicas with different silanol contents and two MFI zeolites with different Al contents. From these measurements, it was found that the silanol groups and Al sites (acid sites) give the significant effect on the nitrogen isotherms at submonolayer, but the argon isotherms are independent from silanols and Al sites. The argon isotherms, therefore, are preferable in calculation of microporosity of zeolites.

Then the argon isotherms for seven zeolites with various micropore size in the pressure range of ($p/p_0=10^{-7}$–0.99) were measured. The zeolites are divided into two groups; Group A zeolites have micropore channels without cage and Group B zeolites have micropore channels with cage. It has been found that the Polanyi adsorption potential of argon atoms for the group A zeolites is closely related with channel size, and that of the group B zeolites depends on both of cage size and channel size.

BELSORP-max can measure vapor adsorption such as water, alcohol, as well. Two series of fluorine-modified catalysts were synthesized. The hydrophobic properties of the catalysts surface were examined by using BELSORP-max and investigated the catalytic performances. By the fluorine-modification, the water adsorption was suppressed and the catalytic reaction was improved. It was found that the fluorine-modification (hydrophobic pretreatment) is effective for improving the catalytic performance.

1.3 References

[1] R. M. Barrer, *J.Soc.Chem.Ind.*, **64**, 130 (1945).

[2] R. M. Barrer, *"Zeolites and Clay Minerals"*, Academic Press, London (1978).

[3] D. W. Breck, W. G. Eversole, R. M. Milton, T. B. Reed, T. L. Thomas, *J. Am. Chem. Soc.,* **78**, 5963 (1956).

[4] H. Yamashita, K. Mori,*Chem. Lett*, **36**, 348 (2007).

[5] H. Yamashita, K. Mori, S. Shironita, Y. Horiuchi, *Catal. Surv. Asia,* **12**, 88 (2008).

[6] K. Kaneko, , H. Tsuchiya, S. Utsumi, T. Ohba, H. Tanaka, H. Kanoh, M. Yudasaka, S. Iijimal, in *Abst. 7th International Symposium on the Characterization of Porous Solids,* p. 27 (2005).

[7] F. Rouquerol, J. Rouquerol, K. S. W. Sing, *"Adsorption by Powders and Porous Solids"*, Academic Press, New York (1999).

Chapter 2

High Precision Volumetric Gas Adsorption Apparatus

2.1 Introduction

Adsorption-desorption isotherms of nitrogen at its boiling point (77K) have been widely used to calculate surface area and porosity of various materials. The volumetric gas adsorption apparatus is useful to measure the nitrogen isotherms. In order to calculate specific surface area with high accuracy and high reproducibility, adsorption isotherms must be measured accurately. In the volumetric method, the amount of adsorption is calculated from state equation of gas (pressure, temperature and volume) and there are a variety of error sources such as dosing volumes, temperature and pressure measurement, sample mass measurements and so on. The estimation of dead volume (*Vd*), free space in the sample container, is important for calculation of adsorption amount in volumetric method. But it is difficult to know the correct *Vd*. One way to determine *Vd* is to measure it before or after the measurement using helium at the measuring temperature and amount of adsorption is calculated under assumption that the *Vd* value is constant during the adsorption measurement. In this case, *Vd* should be kept constant. In another way, *Vd* has to be compensated continuously. There are various ways to determine the *Vd* value. For example:

i). Isothermal jacket method. (Porous material tube)
ii). Dewar elevator method
iii). Vacuum jacket method. (Vacuum sealed sample cell)
iv). LN_2 transfer method
v). Pre-measurement method. (Blank measurement)

In those methods from i) to iv), the liquid nitrogen level in the dewar vessel (LN_2 level) should be kept constant. Various efforts have been made to maintain liquid nitrogen level [1,2]. But it is not easy to maintain LN_2 level without any fluctuations. In addition to that, not only LN_2 level fluctuations but also other factors (room temperature, atmospheric pressure and slight dissolution of oxygen into LN_2) cause change of *Vd*. To keep *Vd* value completely constant is quite difficult.

In the method v), a blank measurement has to be carried out in advance and an isotherm should be measured at the same condition as the blank isotherm is measured. Because all the conditions are not absolutely same in *Vd* measurement and in adsorption measurement, to measure *Vd* change beforehand is not enough correct. A new method to measure *Vd* with a fair degree of precision without controlling LN_2 level was proposed. This method is effective especially in measurement of small surface area sample and reproducibility improves.

2.2 Principle of continuous dead volume measurement

During the adsorption measurement, LN_2 level goes down gradually by evaporation and as a result, Vd gradually decreases. A dVd cell to calculate the Vd changes are (Figure 2-1) was adopted. The dVd cell consists of a cell which has the same inner diameter as the sample cell and a pressure transducer. Prior to the adsorption measurement, a certain amount of helium gas is enclosed into dVd

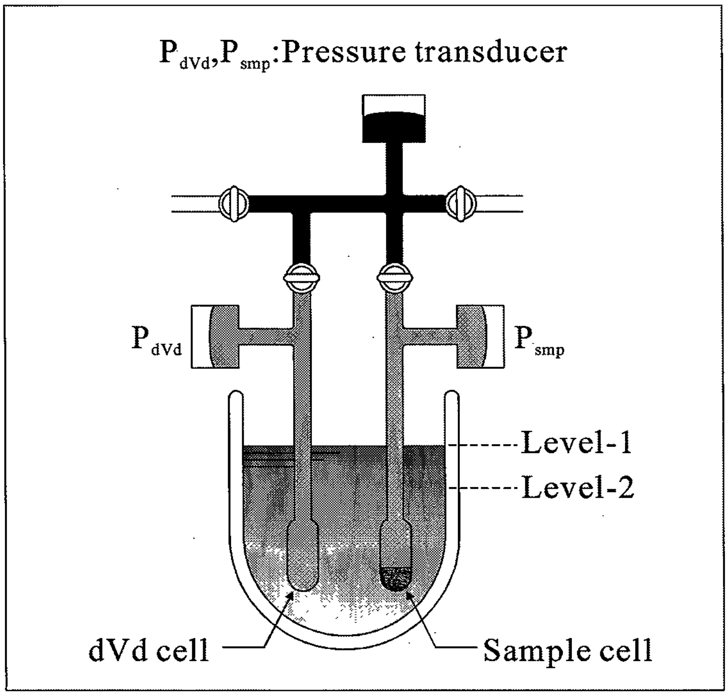

Figure 2-1. Principle of continuous dead volume measurement

cell. Then immerse both cells into LN$_2$. The dead volume of the sample cell is defined as $Vd_{smp}(n)$. In the same way, the dead volume of dVd cell is defined as $Vd_{dVd}(n)$ and the pressure inside dVd cell is defined as $P_{dVd}(n)$. The number in parentheses indicates the LN$_2$ level (Level-1 or Level-2).

$Vd_{dVd}(2)$ is expressed as follows.

$$Vd_{dVd}(2) = Vd_{dVd}(1) \times P_{dVd}(1) / P_{dVd}(2) \tag{1}$$

The variation in Vd_{dVd} when the LN$_2$ level goes down from Level-1 to Level-2(ΔVd_{dvd}) is expressed as follows.

$$\Delta Vd_{dVd} = Vd_{dVd}(2) - Vd_{dVd}(1) \tag{2}$$

Because the inner diameters of dVd cell and the sample cell are the same, Vd_{smp} change equals to ΔVd_{dvd}. As a result $Vd_{smp}(2)$ is expressed as follows.

$$\begin{aligned} Vd_{smp}(2) &= Vd_{smp}(1) + \Delta Vd_{smp} \\ &= Vd_{smp}(1) + \Delta Vd_{dVd} \end{aligned} \tag{3}$$

With our new method (continuous dead volume measurement system), LN_2 level control is not necessary, which leads to a trouble free system and cost savings. Furthermore, Vd is compensated at every step of adsorption measurement precisely, which makes it possible to measure adsorption isotherms with high accuracy and reproducibility. This system is effective especially in measurement of low surface area material.

2.3 Results and discussion

Figure 2-2 shows the pressure transition of dVd cell and the changes in dead volume calculated from it. In the following calculation, a sample cell that has inner diameter of 7mm with filler rod of 6mm in diameter to reduce dead volume was used . Given that LN_2 level is kept to be constant within 1mm, the dead volume error is estimated to 0.073ml. It causes 0.12m^2 of uncertainty in the total surface area calculation. As is described previously, the dead volume uncertainty depends on a variety of factors; hence the surface area error should be considered

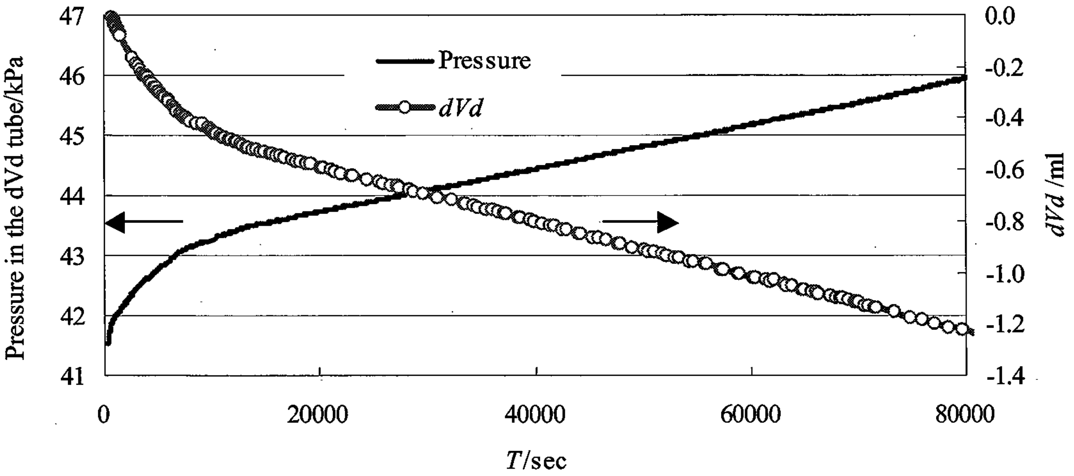

Figure 2-2. Transition of Vd

to be bigger than calculated.

A new adsorption apparatus, BELSORP-mini, which adopts the continuous dead volume measurement system was developed. Isotherms of two certified materials were measured.

1) LGC2102

- Nonporous graphitised carbon black.
- Certified value of nitrogen BET specific surface area is 69±2 m^2 g^{-1}
- Supplied by LGC in UK.

2) CRM-170

- Nonporous alpha alumina
- Certified value of nitrogen BET specific surface area is 1.05±0.05 m^2 g^{-1}
- Supplied by BCR in UK.

Five isotherms of LGC2102 measured with BELSORP-mini are shown all together in Figure 2-3. They coincide well in the whole relative pressure range.

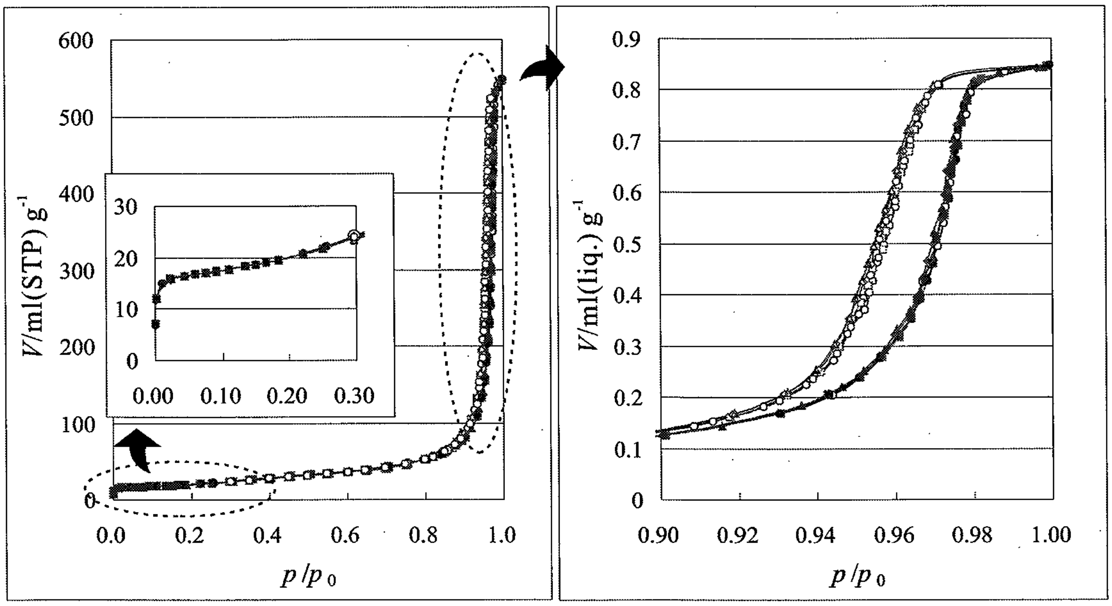

Figure 2-3. Comparison to gas emission amount (pressure increasing) in sample port closed by solenoid valves or pneumatic valves after several hours vacuuming

As is often the case, measurable lower limitation of specific surface area is described to express the specification of an adsorption apparatus but it may be insufficient. It is suggested that reproducibility against the total surface area should be represented for the purpose. Adsorption isotherms of LGC2102 and CRM-170 were measured for estimation of reproducibility.

Adsorption isotherms are measured in different total surface area. These measurements were carried out with using the same sample and the same sample cell repeatedly to avoid the sample weighing error. The total surface area and the reproducibility are shown in Table 2-1 and Figure 2-4. In general, it becomes more difficult to measure nitrogen isotherms on low-area adsorbents (if the specific

Table 2-1. Total surface area and measuring error.

Sample	LGC2102				CRM-170			
Total surface area/m^2	35.2	14.0	7.09	3.94	0.98	0.75	0.12	0.022
No. of measurement	5	5	5	5	10	5	10	9
Error/ %	0.05	0.30	0.33	0.59	1.3	1.77	6.9	36.4

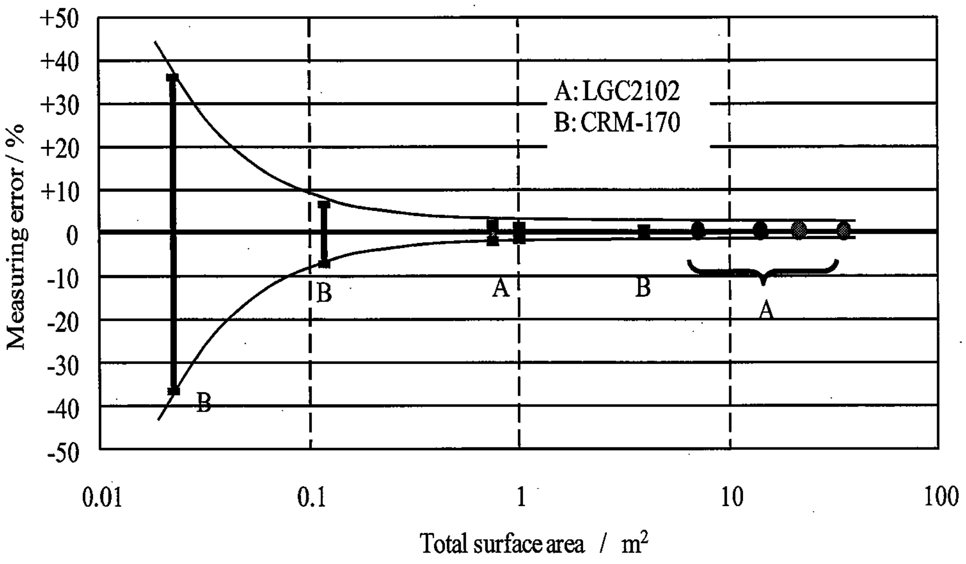

Figure 2-4. Reproducibility against total surface area

surface area<$5m^2$ g^{-1}) in conventional methods [2]. However the new method proposed in this chapter makes it possible to measure low uptakes of gas with high reproducibility (when total surface area>$1m^2$ g^{-1}, measuring error<1.3%). Isotherms of LGC2102 in the relative pressure range from 0.9 to 1.0 are displayed on the right in Figure 2-3. Adsorbed amount are represented as the liquid volume of nitrogen. As described previously, the isotherms coincide well even in the high relative pressure range. It means that the reproducibility of the pore volume is high as well as the specific surface area. According to Gurvitsch rule, the pore volume of LGC2102 (at p/p_0=0.99, pore radius<93nm) was estimated to 0.83cm^3 g^{-1} with STD of 0.003cm^3 g^{-1}. This high reproducibility in high relative pressure range indicates a possibility for analyzing macropore by gas adsorption.

Measuring error is calculated as follows.

$$\text{Measuring error}[\%] = \pm(\text{Standard deviaton}) / (\text{Average of total surface area}) \qquad (4)$$

2.4 Conclusion

In the conventional volumetric method, determining dead volume is quite difficult. Precise LN_2 level control is necessary in some of them. When measuring low surface area material, using krypton gas is desirable instead of nitrogen gas for operational reason. But in using krypton gas, high vacuum system is needed and there are some technical problems.

Comparing to these conventional methods, the new volumetric method;

1. Does not need to maintain LN_2 level.
2. Improves reproducibility both in surface area and in pore volume.
3. Makes it possible to measure adsorption isotherm of low surface area material (e.g. 0.1m^2 in total surface area) without using krypton gas.

2.5 References

[1] H. Naono, K. Nakai, *J. Colloid. Interface Sci.* **128**, 146 (1989).

[2] F. Rouquerol, J. Rouquerol, K. S. W. Sing, *"Adsorption by Powders and Porous Solids"*, Academic Press, New York, 1999.

Chapter 3

Adsorption Isotherm Measurement of N_2 from Extremely Low Relative Pressure (p/p_0=10^{-9}~) to Non-Porous and Microporous Carbon Materials

3.1 Introduction

It is very important for the evaluation of microporous materials to know adsorption behavior under the extremely low-pressure range. Particularly, the experimental isotherm from the low relative pressure gives us more realistic micropore distributions and is useful for the comprehension of the data from a molecular simulation like NLDFT and GCMC. Recent progress of the adsorption apparatus makes it possible to measure the N_2 or Ar adsorption isotherms from the very low pressure such as $p/p_0=10^{-9}$ to the saturation pressure. One of an experimental apparatus to achieve the measurements from the low relative pressure was developed from the Kaneko et al., which was a gravimetric method [1-3]. However, there has ever been no volumetric adsorption technique to get the measurement from the low relative pressure. Hence, BELSORP-max™ has been developed to get easier and more precise isotherms. Besides introductions of feature details of the apparatus, the present chapter consists of the two parts; one is to examine a new standard a_s-data and t-data of non-porous carbon blacks (NPCB) and non-porous graphitised carbon blacks (NPGCB) from the very low relative pressure, and the other is to investigate adsorption isotherm of microporous activated carbon (MPAC) to know the possibilities of measurement errors for porous size distribution and pore volume.

3.2 Adsorption isotherm measurement in extremely low pressure range

The full automatic specific surface area and pore size distribution measurement system (BELSORP-max^{TM}) was developed and the simple process flow diagram is depicted in Figure 3-1. It consists of valves, pressure transducers, vacuum gauges, a turbo molecular pump, a back pump and dedicated software.

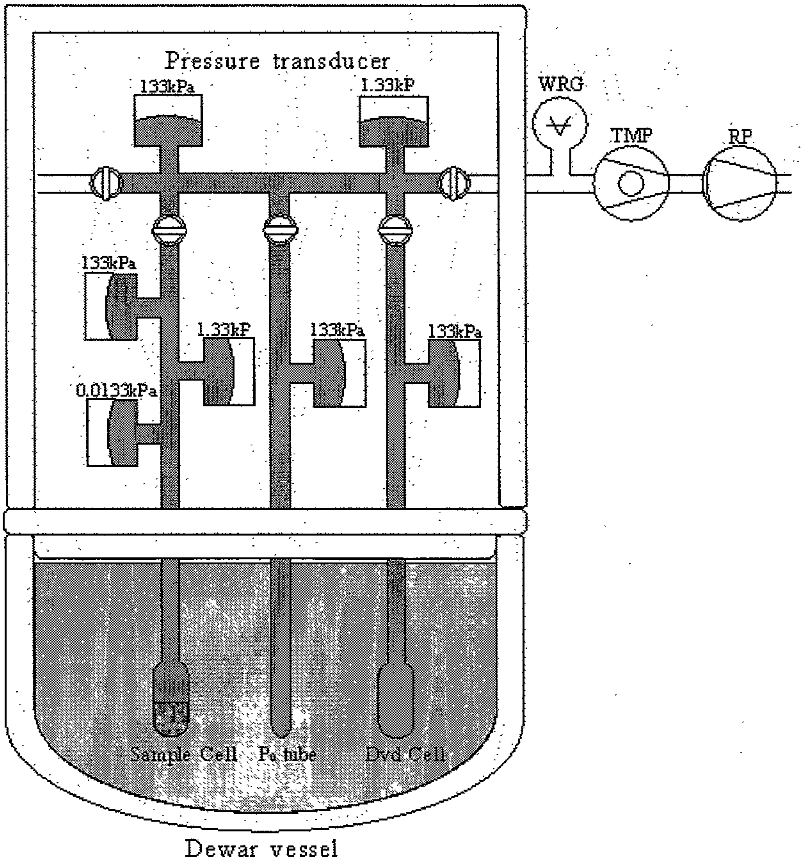

Figure 3-1. Process flow diagram of BELSORP-max^{TM}

The all valves and the transducers are configured in a thermostatic chamber for stable and high resolution measurement. For achievement of the adsorption isotherm measurement through the extremely low relative pressure region (p/p_0=10^{-9}~), there are 5 features in the apparatus. The first is that measurement port has three transducers of 0.0133 kPa, 1.33 kPa and 133 kPa in full scale and can be increased up to 2 ports in maximum. There are two transducers of 1.33kPa and 133kPa in full scale in the standard volume (V_s) part. Besides, it is incorporated another 2 ports for a saturation pressure measurement port with a transducer of 133kPa (P_0 port) and a dead volume (V_d) change measurement port with a transducer of 133kPa (dV_d port for the 2nd feature). So far, the LN_2 level should have been controlled at constant not to occur the V_d change for the accurate isotherm measurement. Continuous dead volume measurement method makes the LN_2 level control unnecessary. The 3rd feature is that piping is used as electrochemical polishing treatment for high ultimate vacuum and the vacuum gauge takes advantage of Pilani gauge with a cold cathode. The ultimate vacuum on sample port was confirmed and the result was achieved 10^{-5} (Pa) order. It is very important for the isotherm measurement from the $p/p_0=10^{-9}$ to keep pressure changes in the equilibrium criteria. Particularly, the considering of emission gas amount form the piping and valves as well as gas permeation amount to the consisted materials in the apparatus is essential and they should be adequately investigated. Hence, the emission gas amount (i.e.; increasing pressure into the cell) from the solenoid valves or pneumatic valves has been examined after vacuuming for several hours as a fundamental study. The results are shown in Figure 3-2. Ultimate vacuum used by pneumatic valves was higher than that by solenoid valves. Comparing the pressure increasing in using solenoid valves to that from pneumatic valves with a specific valve sheet, the latter was 1/500 times smaller than the former. Finally, the pneumatic valves were chosen and were 4th feature in the apparatus. The 5th feature is the dedicated software. The achievement of accurate isotherm measurements must be corrected in the various

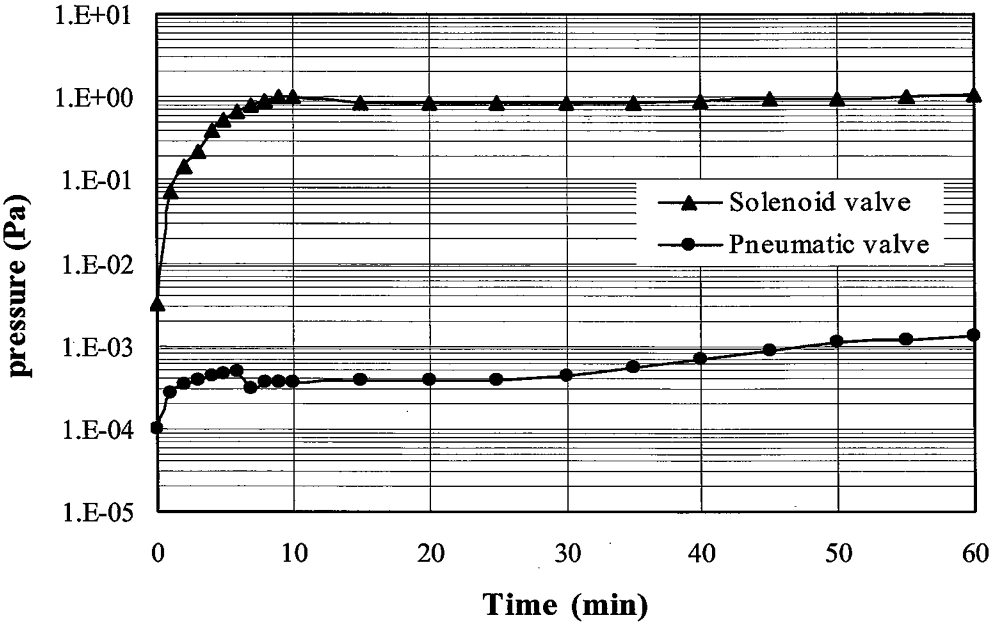

Figure 3-2. Comparison to gas emission amount (pressure increasing) in sample port closed by solenoid valves or pneumatic valves after several hours vacuuming

points of view; thermal transpiration phenomenon at the low relative pressure region and non-ideal gas correction at high relative pressure region. In addition, He adsorption cannot be ignored at such a low pressure region. The dead volume measurement should also be accomplished after the isotherm measurement although it is ordinarily measured before the isotherm measurements. The software is considered the corrections and the He adsorption as just described.

3.3 Experimental

Two kinds of the nonporous carbon were used in this work to investigate the new a_s-data from the low pressure region. The one is the non-porous carbon black

(NPCB) named #51 (Asahi Carbon Co. Ltd.) and the other is the non-porous graphitized carbon black (NPGCB) named LGC2102 supplied by LGC in UK. Prior to the N_2 adsorption, each sample was pretreated at 305°C for 3h in vacuo. A microporous carbon was also used to examine the measurement data from the low pressure region. It is activated carbon (MPAC: AX-21) produced by KOH activations. The carbon sample was pretreated in vacuo at 150℃ for 6h prior to gas adsorption measurement. The high resolution adsorption isotherms of N_2 at 77K (boiling point of liquid nitrogen) from $p/p_0=10^{-9}$ was full-automatically measured by BELSORP-max^{TM}.

3.4 Results and discussion

3.4.1 Standard a_s data and t data of non-porous carbon from extremely low relative pressure

The standard a_s-data and t-data of the non-porous carbon black by Kaneko et al. [1] have been reported in the range between $p/p_0=10^{-4}$ and 0.9. A expanded new standard a_s-data at the range from $p/p_0=10^{-8}$ to 0.9 was investigated. The N_2 adsorption isotherms to NPBC (#51) and NPGCB (LGC2102) were measured at experimental conditions of 77K from $p/p_0=10^{-8}$. The standard a_s-data and t-data are defined as a ratio of the adsorption amount at arbitrary pressure (v_a) to the adsorbed amount at $p/p_0=0.4$ ($v_{0.4}$) and a product of a ratio v_a to adsorbed amount at monolayer (v_m) and adsorption thickness at monolayer (N_2=0.354nm), respectively.

Table 3-1. Standard data of N_2 at 77K for non-porous carbon black (NPCB)

#51(present work)^{*1}			Kaneko et al.^{*2}		#51(present work)^{*1}			Kaneko et al.^{*2}	
p/p_0	t/nm	a_s	t/nm	a_s	p/p_0	t/nm	a_s	t/nm	a_s
8.0E-9	-	2.50E-5	-	-	4.0E-3	-	0.429	-	0.408
1.0E-8	-	8.53E-5	-	-	6.0E-3	-	0.456	-	0.440
2.0E-8	-	3.86E-4	-	-	8.0E-3	-	0.472	-	0.458
4.0E-8		1.00E-3			1.0E-2	0.28	0.478	-	0.472
6.0E-8	-	1.69E-3	-	-	2.0E-2	0.30	0.521	0.27	0.519
8.0E-8	-	2.55E-3	-	-	4.0E-2	0.33	0.572	0.33	0.570
1.0E-7	-	3.46E-3	-	-	6.0E-2	0.34	0.603	0.34	0.602
2.0E-7	-	7.29E-3	-	-	8.0E-2	0.36	0.627	0.36	0.624
4.0E-7	-	1.12E-2	-	-	1.0E-1	0.37	0.649	0.37	0.649
6.0E-7	-	1.41E-2	-	-	1.5E-1	0.40	0.704	0.41	0.710
8.0E-7	-	1.65E-2	-	-	2.0E-1	0.43	0.759	0.44	0.768
1.0E-6	-	1.86E-2	-	-	2.5E-1	0.47	0.816	0.47	0.827
2.0E-6	-	2.62E-2	-	-	3.0E-1	0.50	0.875	0.51	0.887
4.0E-6	-	3.66E-2	-	-	3.5E-1	0.54	0.938	0.54	0.950
6.0E-6	-	4.41E-2	-	-	4.0E-1	0.57	1.000	0.57	1.000
8.0E-6	-	4.92E-2	-	-	4.5E-1	0.61	1.031	0.61	1.068
1.0E-5	-	5.43E-2	-	-	5.0E-1	0.64	1.126	0.64	1.128
2.0E-5	-	7.37E-2	-	-	5.5E-1	0.68	1.193	0.68	1.198
4.0E-5	-	9.93E-2	-	-	6.0E-1	0.72	1.267	0.72	1.266
6.0E-5	-	0.117	-	-	6.5E-1	0.77	1.350	0.77	1.340
8.0E-5	-	0.132	-	-	7.0E-1	0.83	1.446	0.80	1.408
1.0E-4	-	0.145	-	0.107	7.5E-1	0.89	1.564	0.85	1.482
2.0E-4	-	0.192	-	0.206	8.0E-1	0.98	1.717	0.90	1.570
4.0E-4	-	0.249	-	0.232	8.5E-1	1.10	1.932	0.96	1.680
6.0E-4	-	0.284	-	0.259	8.75E-1	1.19	2.084	0.99	1.737
8.0E-4	-	0.310	-	0.278	9.0E-1	1.31	2.298	1.02	1.795
1.0E-3	-	0.328	-	0.292	9.2E-1	1.46	2.547	1.07	1.880
2.0E-3	-	0.363	-	0.371	9.4E-1	1.70	2.974	1.12	1.970

*1) #51: 18.88m^2/g, (C_{BET}=158)

*2) Kaneko et al.: 81.00m^2/g, (C_{BET}=300)

Table 3-2. Standard data of N_2 at 77K for non-porous graphitized carbon black (NPGCB^{*3})

p/p_0	t/nm	a_s	p/p_0	t/nm	a_s	p/p_0	t/nm	a_s
2.0E-8	-	3.06E-5	8.0E-5	-	9.10E-2	2.0E-1	0.44	0.723
4.0E-8	-	2.13E-4	1.0E-4	-	0.110	2.5E-1	0.48	0.789
6.0E-8	-	5.99E-4	2.0E-4	-	0.205	3.0E-1	0.53	0.869
8.0E-8	-	9.45E-4	4.0E-4	-	0.327	3.5E-1	0.59	0.955
1.0E-7	-	1.24E-3	6.0E-4		0.384	4.0E-1	0.63	1.034
2.0E-7	-	2.11E-3	8.0E-4	-	0.413	4.5E-1	0.68	1.105
4.0E-7	-	2.92E-3	1.0E-3	-	0.433	5.0E-1	0.72	1.172
6.0E-7	-	3.51E-3	2.0E-3		0.476	5.5E-1	0.76	1.242
8.0E-7	-	4.02E-3	4.0E-3	-	0.504	6.0E-1	0.81	1.321
1.0E-6	-	4.49E-3	6.0E-3	-	0.520	6.5E-1	0.87	1.416
2.0E-6	-	6.48E-3	8.0E-3	-	0.529	7.0E-1	0.94	1.535
4.0E-6	-	9.77E-3	1.0E-2	0.33	0.537	7.5E-1	1.04	1.689
6.0E-6	-	1.27E-2	2.0E-2	0.34	0.559	8.0E-1	1.17	1.907
8.0E-6	-	1.54E-2	4.0E-2	0.36	0.584	8.5E-1	1.37	2.241
1.0E-5	-	1.80E-2	6.0E-2	0.37	0.601	8.75E-1	1.54	2.517
2.0E-5	-	2.98E-2	8.0E-2	0.38	0.616	9.0E-1	1.76	2.874
4.0E-5	-	5.10E-2	1.0E-1	0.39	0.631	9.2E-1	2.09	3.403
6.0E-5	-	7.13E-2	1.5E-1	0.41	0.674	9.4E-1	2.65	4.323

*3)LGC2102: 70.98 (m^2/g) (C_{BET}=695)

The specific surface area and C constant of NPBC and NPGCB were respectively 18.88 (m^2/g) (C_{BET}=156) and 70.98 (m^2/g) (C_{BET}=695). The results of NPBC and NPGCB were shown in Table 3-1 and 3-2. The former data includes results from p/p_0=10^{-4} by Kaneko et al. for more rigorous discussion. Besides these tables, the a_s-data and t-data of the three materials were summarized in Figure 3-3 and 3-4. The a_s-data of NPCB (#51) from p/p_0=10^{-4} to p/p_0=0.75 were good agreement with those of NPCB$_K$ although the results from 0.75 to 0.9 of p/p_0 were just a little bit different.

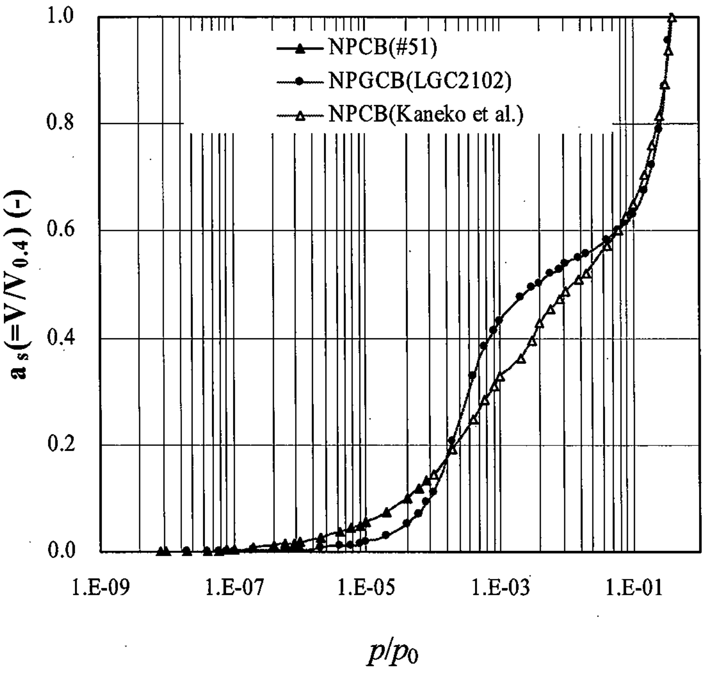

Figure 3-3. Standard α_s-curve of N_2 at 77K for NPCB and NPBC

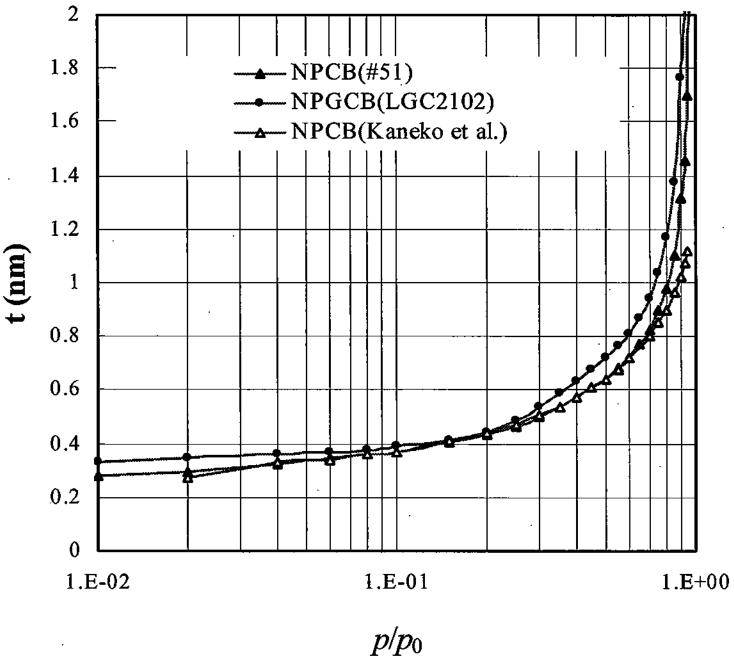

Figure 3-4. Standard t-curve of N_2 at 77K for NPCB and NPGCB

The reasons probably come from tiny hysteresis between adsorption and desorption branches in the isotherm, which it does not come from existing pores in the material but come from void between particles because of using couple of micron ordered powders. According to the experimental isotherm, it was evident that the shape of isotherm was clearly type II isotherm up to 0.75 of p/p_0. Contrary to data mismatching at high relative pressure, the new obtained data from $p/p_0=10^{-8}$ to $p/p_0=10^{-4}$ will be more effective to know the information of microporous carbon materials. Similarly the a_s-data of NPCB, the obtained t-data from 0.01 to 0.75 of p/p_0 also agreed well with those of the $NPCB_K$ as shown in Figure 3-4. It was found that the a_s-data of NPGCB was more specific than that of NPGC in Figure 3-3, which had step shape isotherm at around 0.4 of a_s. This phenomenon is referable to homogeneity of the carbon surface. In other words, it seems that the graphitized surface of NPGCB is more than that of NPCB.

3.4.2 Comparison of pore size distribution of MPAC isotherm from $p/p_0=10^{-9}$ to that from $p/p_0=10^{-6}$

The two high resolution adsorption isotherms for MPAC (AX-21) was obtained at 77K of N_2 from $p/p_0=10^{-9}$ and from $p/p_0=10^{-6}$ to compare the pore size distribution and pore volume at the each measurement. The results from $p/p_0=10^{-9}$ and from $p/p_0=10^{-6}$ were shown in Figure 3-5 and 3-6, respectively. Both results were agreed well from $p/p_0=10^{-6}$ and gave us the information of existence of micropores and mesopores because there were two increasing points of adsorbed

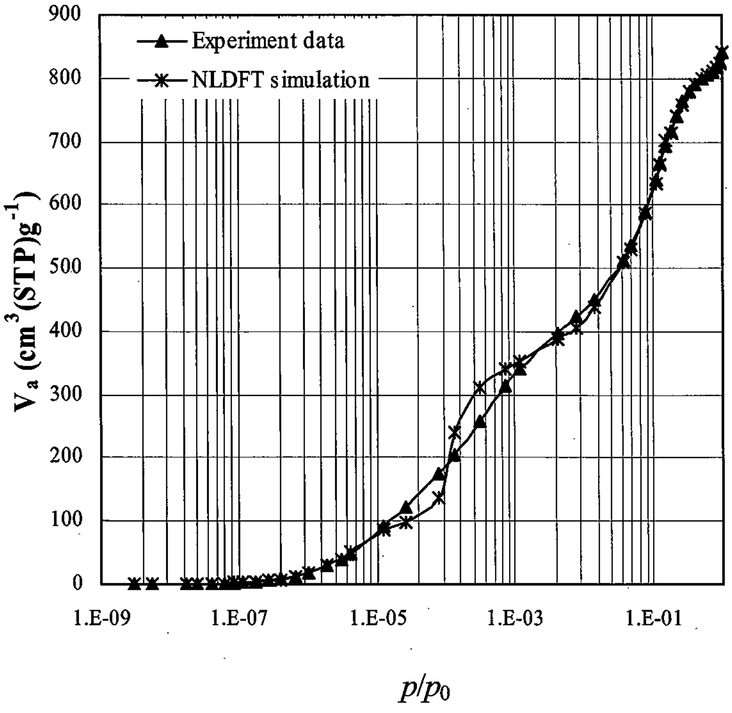

Figure 3-5. Adsorption isotherm of N_2 at 77K from $p/p_0 = 10^{-9}$ for MPAC

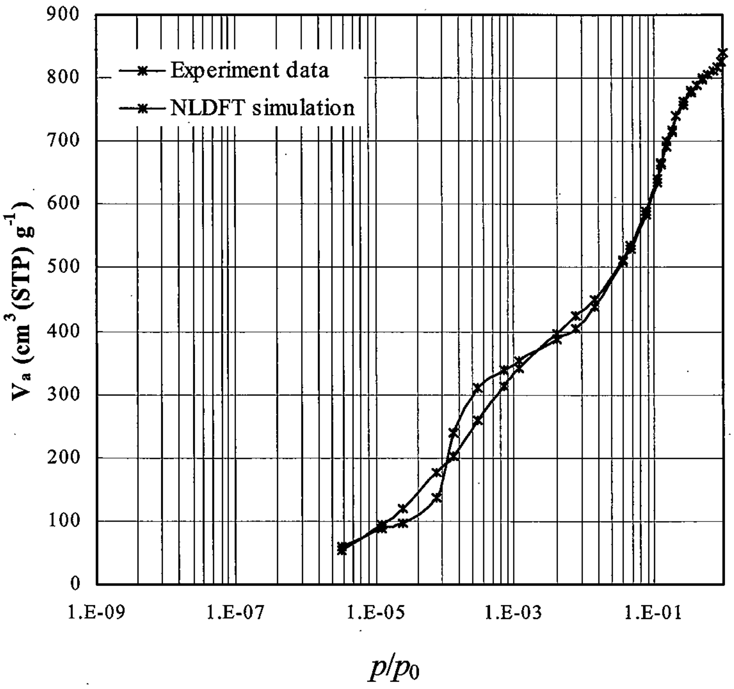

Figure 3-6. Adsorption isotherm of N_2 at 77K from $p/p_0 = 10^{-6}$ for MPAC

amount at around $p/p_0=10^{-3}$ and $p/p_0=0.1$.

However, it seems that there is some differences of results for the pore size distribution (PSD) and pore volume because the isotherm from Figure 3-6 was short of the data from $p/p_0=10^{-9}$ to $p/p_0=10^{-6}$. Hence, it is discussed that how much difference in this section. The PSD and pore volume from obtained each isotherm were calculated from HK method for micropores, BJH method for mesopores and NLDFT for both pores by BELMaster™. PSD from NLDFT is calculated from model isotherms under the basis of assumption of homogeneity carbon surface with slit shape pore. The obtained isotherms from NLDFT were also drawn in Figure 3-5 and 3-6. Besides, the PSD from $p/p_0=10^{-9}$ and $p/p_0=10^{-6}$ were shown in the Figure 3-7 and 3-8. The results of pore diameter peaks (d_p) and pore volumes (V_p) from three calculations were summarized in Table 3-3. The pore diameter position from the each isotherm didn't change at all. On the other side, PSD curve was different because of the lack of data numbers from $p/p_0=10^{-9}$ and $p/p_0=10^{-6}$ as expected. Particularly, the difference of the pore volume calculated from $p/p_0=10^{-9}$ and $p/p_0=10^{-6}$ was just about 0.007 (cm^3/g). In other words, the differences have possibility around 0.5% PSD measurement error as seen in the Table 3-3. The isotherm measurement from the extremely low relative pressure could be given more accurate and rigorous information for microporous materials from these points of views.

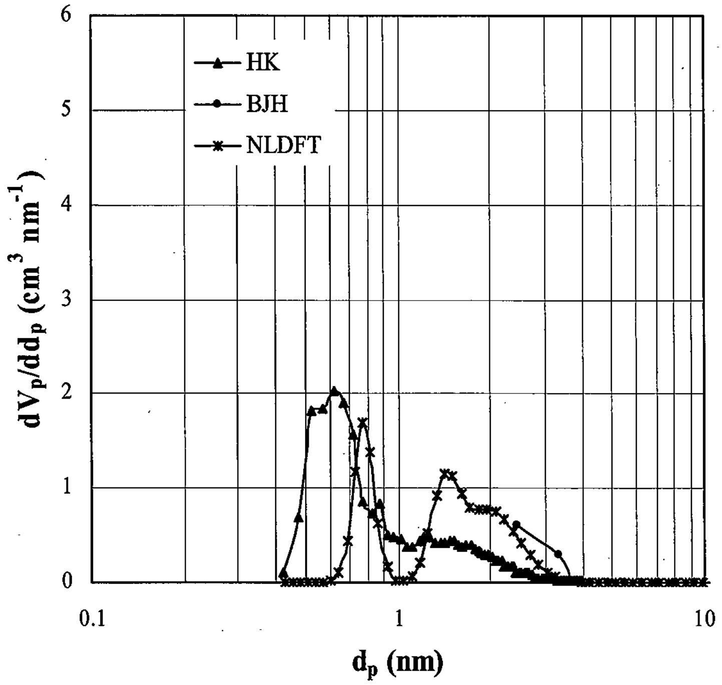

Figure 3-7. PSD calculation from various analysis methods (p/p_0=10^{-9} ~)

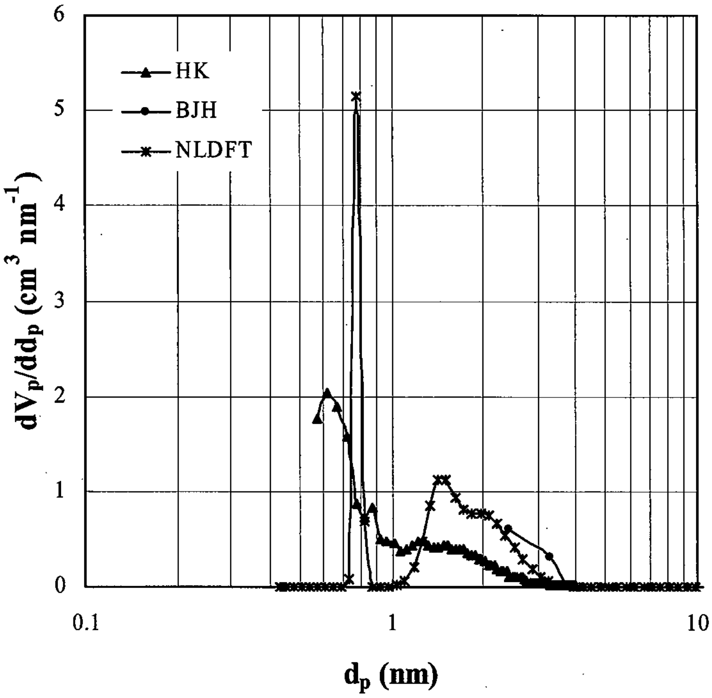

Figure 3-8. PSD calculation from various analysis methods (p/p_0=10^{-9} ~)

Table 3-3. Comparison of pore diameter (d_p) peak position and pore volume (V_p) of MPAC by isotherm measurement of N_2 at 77K from $p/p_0=10^{-9}$ to that from $p/p_0=10^{-6}$

Meas. range	-	NLDFT		HK	BJH
$p/p_0=10^{-9}$~	d_p peak (nm)	0.7671	1.51	0.62	2.43
	V_p (cm^3/g)	1.5487		1.2216	0.401
$p/p_0=10^{-6}$~	d_p peak (nm)	0.7671	1.51	0.62	2.43
	V_p (cm^3/g)	1.5410		1.2216	0.401

3.5 Conclusions

The new volumetric adsorption isotherm measurement apparatus with many features for extremely low pressure was developed, which could measure from $p/p_0=10^{-9}$ and obtained high resolution, reproducibility and repeatability. The new standard a_s data for NPCB and NPGCB that could not have achieved because of the low ultimate pressure was given from $p/p_0=10^{-8}$. Accordingly, more important information for microporous material would be given by the isotherms. MPAC was also measured to confirm that how much PSD and pore volume was changed by difference of measurement range of 10^{-9} and 10^{-6}. It quantitatively confirmed around 0.5% PSD measurement error. Finally, it was proved that the isotherm measurement from the extremely low relative pressure could be given more accurate and rigorous information for microporous materials.

3.6 References

[1] Kaneko, K., H. Tsuchiya, S. Utsumi, T. Ohba, H. Tanaka, H. Kanoh, M. Yudasaka, S. Iijimal, *Abst. 7th International Symposium on the Characterization of Porous Solids*, p.27 (2005).

[2] Rouquerol, F., Rouquerol, J., Sing, K. S. W. *"Adsorption by Powders and Porous Solids"*, Academic Press, New York (1999).

[3] H. Naono, K. Nakai, *J. Colloid. Interface Sci.*, **128**, 146 (1989).

Chapter 4

High Resolution Argon Adsorption Isotherms for Various Zeolites

4.1 Introduction

The microporosity of zeolite channels or cages has been extensively investigated using the N_2 adsorption isotherms at 77.4 K [1]. It is a well-known fact that the N_2 molecule is specific adsorptive having quadrupole moment [2], where the specific interaction between quadrupole moment of N_2 molecule and functional groups on solid surface or charges in zeolite channels may occur in N_2 adsorption. On the other hand, the Ar atom is nonspecific adsorptive [2], where van der Waals interaction is the main factor in the Ar adsorption, and the surface functional groups or charges in channels may have little influence on the Ar isotherms. The present results show clearly that silanol groups on silicas or protons in zeolite channels have an appreciable effect on the N_2 isotherm, but have little influence on the Ar isotherms. Accordingly, the Ar isotherms at 87.3 K have been used in study of microporosity of zeolites.

Recent progress of the adsorption apparatus makes it possible to measure the adsorption isotherms of N_2 and Ar from very low relative pressure such as $p/p_0=10^{-9}$ to saturation vapor pressure. Accordingly, it is able to examine the adsorption behavior of N_2 or Ar from very low coverage in details. The adsorption behavior of Ar and N_2 trapped in the micropore channels of MFI zeolites has been reported [3-6]. In the present work, the adsorption isotherms of Ar atoms at 87.3 K have been measured for the various zeolites with different channel size or different cage size. On the basis of the Ar adsorption isotherms, the relation between adsorption potential of Ar atoms and channel size or cage size has been examined.

4.2 Experimental

Table 4-1. Zeolite samples.

Group	Type	Ring number	Pore size / Å	
			channel	
A	MFI (ZSM-5)	10	5.1×5.5 ; 5.3×5.6	
	MTW (ZSM-12)	12	5.6×6.0	
	AFI (SSZ-24)	12	7.3	
	AFI (AlPO-5)	12	7.3	
	VFI (VPI-5)	18	12.7	
			Window	Cage
B	LTA (Type A-Ca)	8	5	11
	FAU (Type Y)	12	7.4	13

The zeolite samples used in this work are listed in Table 4-1, in which the ring number, pore size are shown. Two samples of MFI zeolites (ZSM-5; $SiO_2/Al_2O_3=1000$, $SiO_2/Al_2O_3=25$) are the reference materials of Catalysis Society of Japan (JRC-Z5-1000H, JRC-Z5-25H). Four samples of MTW(ZSM-12), AFI(SSZ-24), AFI(AlPO-5), and VFI(VPI-5) were supplied from Prof. Y. Kubota of Yokohama National University. LTA (Type A-Ca) and FAU (Type Y) are the reference materials of European Commission Directorate-General Joint Centre (BCR-705 and BCR-704).

Prior to gas adsorption measurement, the zeolite samples were pretreated in vacuo at 623 K for 10 h. The adsorption isotherms of Ar at 87.3 K (boiling point of liquid argon) and of N_2 at 77.4 K (boiling point of liquid nitrogen) were measured by BELSORP-max, which has three pressure transducers of 0.0133 kPa, 1.33 kPa and 133 kPa in full scale. Using these transducers, it is possible to measure the adsorption isotherm of Ar or N_2 from $p/p_0=10^{-9}$ to saturation pressure. All isotherms measured by BELSORP-max are changed into the a_s-curve (*cf.* Figures. 4-1 ~ 4-4), where a_s is defined as $v_a/v_{0.4}$ (V_a : adsorbed amount at arbitrary pressure, and $v_{0.4}$: adsorbed amount at $p/p_o=0.4$).

4.3 Results and discussion

4.3.1 Effect of silanols on surface or protons in channels for adsorption isotherms of Ar (87.3 K) and N_2 (77.4 K)

Prior to investigation of microporosity of zeolites, the effect of silanol groups of nonporous silicas and protons of zeolite channels on the adsorption behavior of Ar (87.3 K) and N_2 (77.4 K) were examined.

The effect of surface silanol groups on the Ar and N_2 isotherms was investigated at first. The high resolution adsorption isotherms of Ar (87.3 K) and N_2 (77.4 K) on hydroxylated and dehydroxylated nonporous silicas (Aerosil-200) are shown in Figure 4-1(a) and 1(b). The hydroxylated silica has the silanol group of 3.3 OH/nm^2, while the dehydroxylated silica has the silanol group of 0.35 OH/nm^2. These

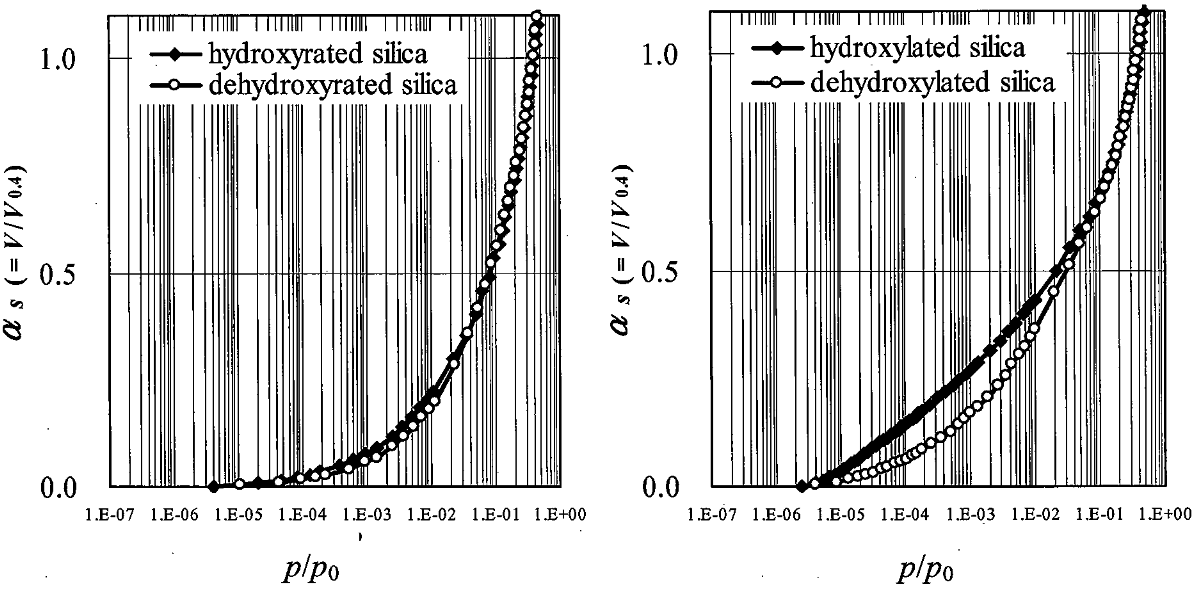

Figure 4-1. High resolution adsorption isotherms for nonporous silicas ; (a) Ar isotherms at 87.3 K (b) N_2 isotherms at 77.4 K.

surface silanol contents were evaluated on the basis of the adsorption isotherms of water vapor (298.1 K) for the hydroxylated silica (A_{BET}=188 m^2/g) and the dehydroxylated silica (A_{BET}=168 m^2/g). Figure 4-1(a) and 1(b) clearly indicate that the silanol groups have little influence on the Ar isotherm, but give an appreciable effect on the N_2 isotherms below a_s=0.5.

The effect of charge in zeolite channels on the Ar and N_2 isotherms has been investigated using two MFI zeolites of (Si/Al)=500 and (Si/Al)=12.5. The high resolution isotherms of Ar (87.3 K) and N_2 (77.4 K) on these two zeolites are shown in Figure 4-2(a) and 4-2(b), whose results clearly indicate that the proton content in zeolite channels have little influence on the Ar isotherm, but the significant effect was

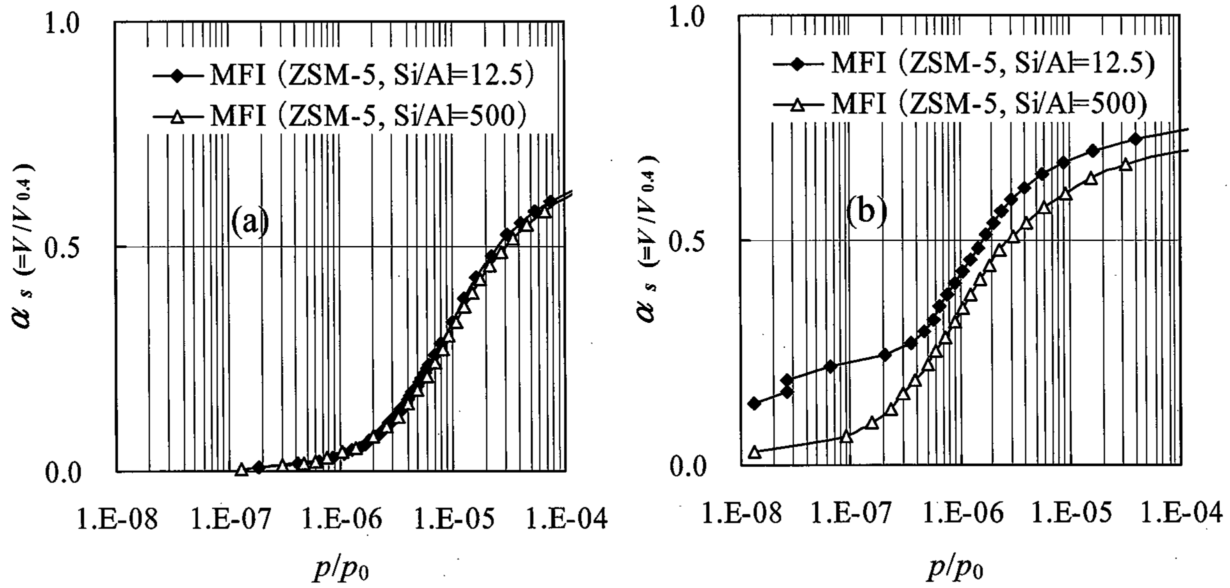

Figure 4-2. High resolution adsorption isotherms for MFI zeolites ; (a) Ar isotherms at 87.3 K (b) N_2 isotherms at 77.4 K.

observed in the N_2 isotherms. It is evident from the present results (Figure 4-1 and 4-2) that the Ar isotherm is almost independent of the surface groups or the channel charge. In this work, therefore, the Ar isotherms are used in evaluation of microporosity of various zeolites having different channel or cage size.

4.3.2 Evaluation of microporosity of zeolites on the basis of high resolution adsorption isotherms of Ar (87.3 K)

The high resolution adsorption isotherms of Ar (87.3 K) for the group A zeolites are shown in Figure 4-3 (a) and (b). From the Ar isotherms of Figure 4-3 and the channel size in Table 4-1, it is found that the Ar isotherms for the group A zeolites shift to higher relative pressure with increase of channel size. The unique jump in the Ar isotherm for MFI zeolite is observed near $p/p_0=10^{-3}$, whose phenomenon may be related to the phase transition of Ar atoms trapped in the MFI zeolite channels [4-6].

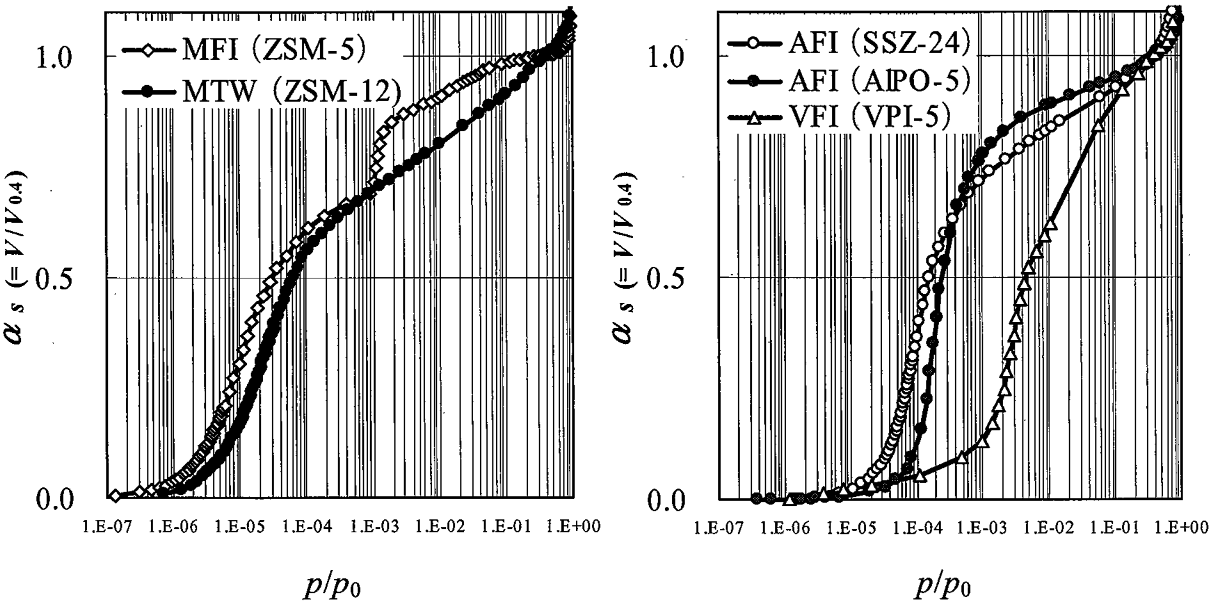

Figure 4-3. High resolution Ar adsorption isotherms at 87.3 K for zeolites of group A.

In the cases of AFI(SSZ-24) and AFI(AlPO-5), their channel size is same, but the Ar isotherms for these zeolites are slightly different one another. Such difference in the Ar isotherms may be related to difference in chemical compositions (SSZ-24=SiO_2, AlPO-5=$AlPO_4$). The high resolution adsorption isotherms of Ar (87.3 K) for the group B zeolites are shown in Figure 4-4. From the Ar isotherms of Figure 4-4 together with cage size in Table 4-1, it is found that the Ar isotherms for the group B zeolites shift to higher relative pressure with increase of cage size.

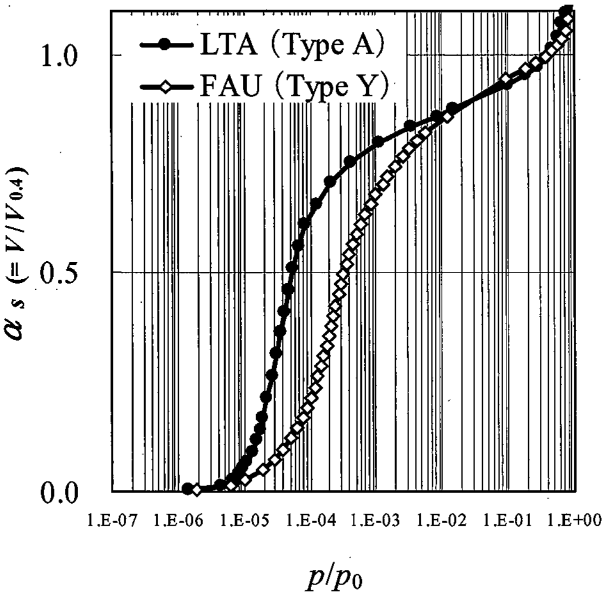

Figure 4-4. High resolution Ar adsorption isotherms at 87.3 K for zeolites of group B.

On the basis of the Ar adsorption isotherms given in Figure 4-3 and 4-4, the Polanyi adsorption potential ($A=RT\ln(p/p_0)$ at a_s=0.5 was evaluated for each zeolite. The Polanyi adsorption potential is the depth of the potential well of channel or cage in zeolite [7]. a_s=0.5 corresponds to the situation that the channel or cage is half-filled with the adsorbed Ar atoms. The Polanyi adsorption potentials expressed as

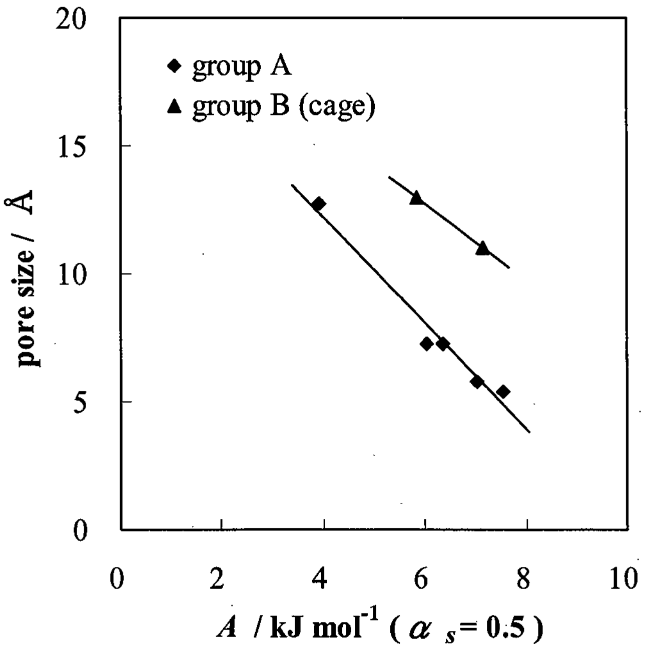

Figure 4-5. Polanyi adsorption potentials vs. pore size or cage size of zeolites.

kJ/mol are plotted against pore size or cage size of zeolites, whose result is shown in Figure 4-5.

For the group A zeolites, the following equation is obtained:

$$A = -2.07 + 20.50 \times d \quad (d\text{ : channel diameter expressed as Å}) \qquad (1)$$

For the group B zeolites, only two zeolites are examined. The tentative equation may be given in the present work; more data for different cage size must be accumulated in future.

$$A = -1.51 + 21.80 \times d \quad (d\text{ : cage diameter expressed as Å}) \qquad (2)$$

The Ar adsorption data given in the present work play an important role for evaluation of pore size distributions of zeolites from Non-local Density Functional Theory (NLDFT) and from Grand Canonical Monte Carlo simulation method (GCMC).

4.4 Conclusion

The number of silanol groups has little influence on the Ar isotherm, but give an appreciable effect on the N_2 isotherms below a_s=0.5. Also, the proton content in zeolite channels has little influence on the Ar isotherm, but the significant effect was observed in the N_2 isotherms. Therefore, the Ar isotherms should be used in evaluation of microporosity of various zeolites having different channel or cage size.

Argon high resolution isotherms at 87.3K are measured for a variety of zeolites and found the relationship between Polani adsorption potential and the pore size. In case of zeolites without cage, the adsorption potential depends on the channel size. On the other hand, the adsorption potential can be determined by the cage size for zeolites with cage.

4.5 References

[1] R. Rouquerol, J. Rouquerol, K. Sing, *"Adsorption by Powder and Porous Solids"*, Academic Press, San Diego, p. 378 (1999).

[2] S. J. Gregg, K. S. W. Sing, *"Adsorption, Surface Area and Porosity"*, Academic Press, London, p. 11. (1982).

[3] K. Nakai, M. Hakuman, H. Naono, *Zeolites News Letters*, **23**, 2 (2006).

[4] K. Nakai, M. Hakuman and H. Naono, *Abst. The 4th Pacific Basin Conference on Adsorption Science and Technology*, A6, May 22-26, China (2006)

[5] K. Nakai, M. Hakuman, H. Naono, *Abst. The 5th Tokyo Conference on Advanced Catalytic Science and Technology*, p. 418 (2006).

[6] K. Nakai, M. Hakuman, H. Naono, *Abst. The International Symposium on Zeolites and Microporous Crystals*, p. 2046, (2006).

[7] S. J. Gregg, K. S. W. Sing, Adsorption, "*Surface Area and Porosity*", Academic Press, London, p. 220. (1982).

Chapter 5

High Resolution Adsorption Isotherms of N_2 and Ar for Nonporous Silicas and MFI Zeolites

5.1 Introduction

Recent progress of the adsorption apparatus makes it possible to measure the N_2 and Ar adsorption isotherms from $p/p_0=10^{-8}$ to 0.998 [1, 2]. Accordingly, it is able to evaluate the adsorption behavior of these adsorbates in detail from submonolayer to multilayer; namely, $a_s=0.01$ – 8. The present work consists of the two parts; one is to examine effect of silanol groups of silica or acid sites of MFI zeolites on the high resolution adsorption isotherms of N_2 and Ar at their boiling points, and the other is to investigate the differential adsorption energy of N_2 and Ar with the micropore channels of MFI zeolite from micropore filling as low as $a_s=0.1$. In the present work, it is shown that the high resolution isotherms of N_2 and Ar give important information about characterization of silica surface and channel surface of microporous MFI zeolite.

5.2 Experimental

Two kinds of the nonporous silicas were used in this work. The hydroxylated silica was prepared by immersing fine silica particles (Aerosil-200) in distilled water, while the dehydroxylated silica was prepared by heating hydroxylated silica at 1000℃ for 4 h *in vacuo.* Prior to the N_2 or Ar adsorption, the silica samples were pretreated at 110℃ for 4 h *in vacuo.* The silanol contents of the two silicas were evaluated from the BET monolayer value of the water isotherm at 25℃ [3]. Two samples of MFI zeolites ($SiO_2/Al_2O_3=1000$, $SiO_2/Al_2O_3=25$) were the reference materials of Catalysis Society of Japan (JRC-Z5-1000H, JRC-Z5-25H). MTW (ZSM-12) was kindly supplied from Y. Kubota of Yokohama National University. Prior to gas adsorption measurement, the zeolite samples were pretreated in vacuo at 350℃ for 10 h.

The high resolution adsorption isotherms of N_2 at 77.4 K (boiling point of liquid nitrogen) and Ar at 87.3 K (boiling point of liquid argon) were measured by BELSORP-max, which has three pressure transducers of 0.0133 kPa, 1.33 kPa and 133 kPa in full scale. Using these transducers, it is possible to measure the adsorption isotherm of N_2 or Ar from $p/p_0=10^{-9}$ to saturation pressure. The Ar isotherm at 94 K was measured by the volumetric adsorption apparatus (BELCryo), in which the cryostat is incorporated.

The N_2 and Ar isotherms measured by BELSORP-max are changed into the α_s -curve, where α_s is defined as $V_a/V_{0.4}$ (V_a: adsorbed amount at arbitrary pressure, and $V_{0.4}$: adsorbed amount at $p/p_0=0.4$).

5.3 Results and discussion

5.3.1 High resolution adsorption isotherms of N_2 and Ar for nonporous silicas and microporous MFI zeolites at their boiling points

Figures 5-1(a) and 5-1(b) show the high resolution adsorption isotherms of N_2 (77.4 K) and Ar (87.3 K) for the hydroxylated silica (A_{BET}=188 m^2/g) and the dehydroxylated silica (A_{BET}=168 m^2/g) whose silanol content was evaluated to be 3.3 OH/nm^2 and 0.35 OH/nm^2, respectively. The results shown in Figure 5-1(a) and Figure 5-1(b) clearly indicate that the N_2 isotherms at the submonolayer range (a_s= 0.01–0.5) have different patterns for the two silicas, while the two Ar isotherms almost overlap one another below a_s=1.0. It is evident that the surface silanol groups give a significant effect on the N_2 isotherms below a_s=0.5, but the silanols give little influence on the Ar isotherms.

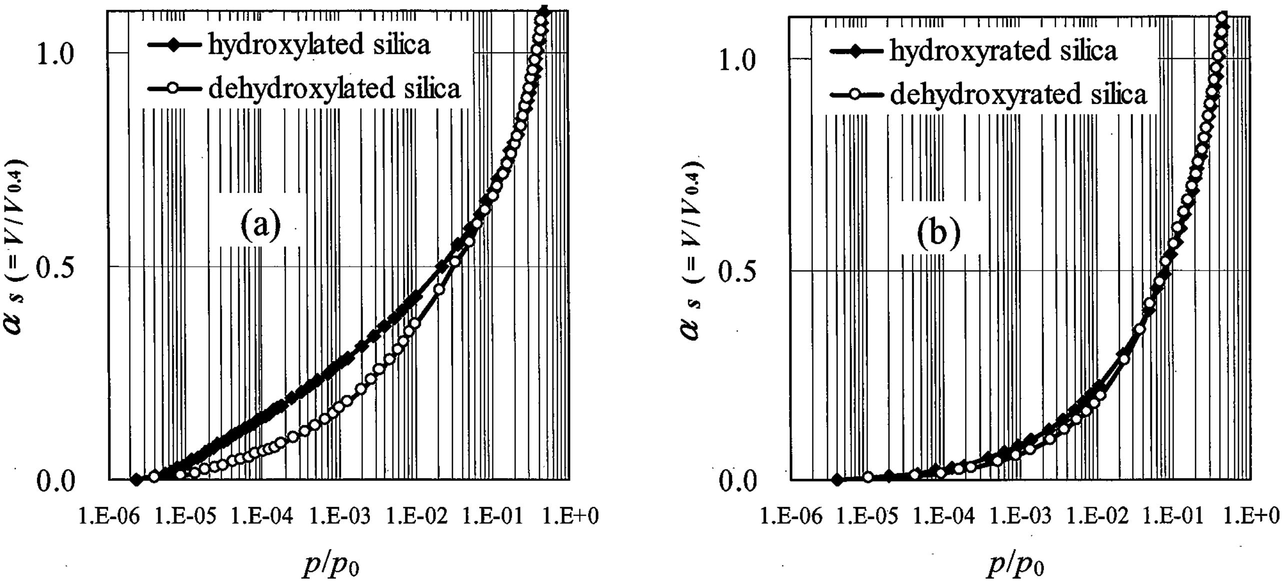

Figure 5-1. High resolution adsorption isotherms for nonporous silicas ; (a) N_2 isotherms at 77.4 K (b) Ar isotherms at 87.3 K.

Figures 5-2(a) and 5-2(b) show the high resolution adsorption isotherms of N_2 (77.4 K) and Ar (87.3 K) for the two kinds of microporous MFI zeolites in which the ratio of Si/Al is 12.5 and 500, respectively. At the submonolayer coverage (a_s=0.01–0.6), the two Ar isotherms almost overlap one another (*cf.* Figure 5-2(b)), but there is remarkable difference in the two N_2 isotherms below a_s=0.25 (*cf.* Figure 5-2(a)). It is shown that the MFI sample having a large Al content (Si/Al=12.5) gives large effect for the N_2 isotherms; in other words, the Al sites (*i.e.,* acid sites) in MFI zeolite give a significant influence on

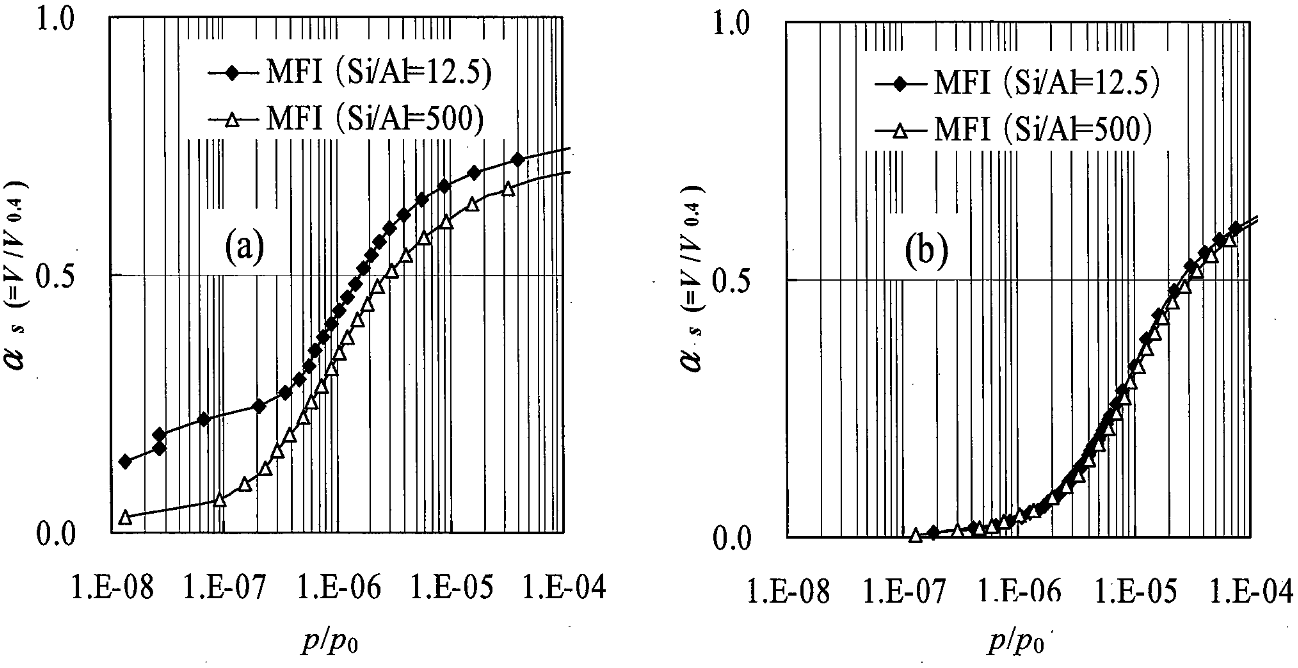

Figure 5-2. High resolution adsorption isotherms for MFI zeolites ; (a) N_2 isotherms at 77.4 K (b) Ar isotherms at 87.3 K.

the N_2 adsorption isotherms.

The experimental facts found in the silica samples and in the MFI samples are closely correlated with the molecular characters of N_2 and Ar. It is well-known that the N_2 molecule is specific adsorptive having quadrupole moment, while Ar atom is nonspecific adsorptive where van der Waals force is the main factor in the Ar adsorption [4]. The present adsorption data given in Figure 5-1 and 5-2 indicate that the interaction of the quadrupole moment of nitrogen molecule with the silanol group on the nonporous silica surface or with the Al-sites (acid sites) present in the microporous channels of MFI zeolites can be detected in their adsorption isotherms in the submonolayer range.

The high resolution Ar isotherms are preferable for calculation of microporosity of zeolites, because the Ar adsorption isotherms from $p/p_0=10^{-7}$ to $p/p_0=10^{-4}$ are independent of the Al content of zeolites. In Figure 5-3, the pore size distribution of the two MFI zeolites having Si/Al=12.5 and Si/Al=500 were calculated by the Grand Canonical Monte Carlo simulation method (BELSim) developed by BEL JAPAN, Inc., where the Ar isotherms given in Figure 5-2(b) were used. The two zeolites [MFI (Si/Al=12.5) and MFI (Si/Al=500)] give the same peak position of d_p=0.56 nm, whose pore size corresponds to the channel size of MFI zeolite shown in Figure 5-4. The minute peak near d_p=1 nm, which arises from the step of the Ar isotherm in the vicinity of $p/p_0=10^{-3}$ (*cf.* Figure 5-5(a)). Similar calculation was carried out using the N_2 isotherm (*cf.* Figure 5-5(a)). The main peak appears at d_p=0.56 nm, but

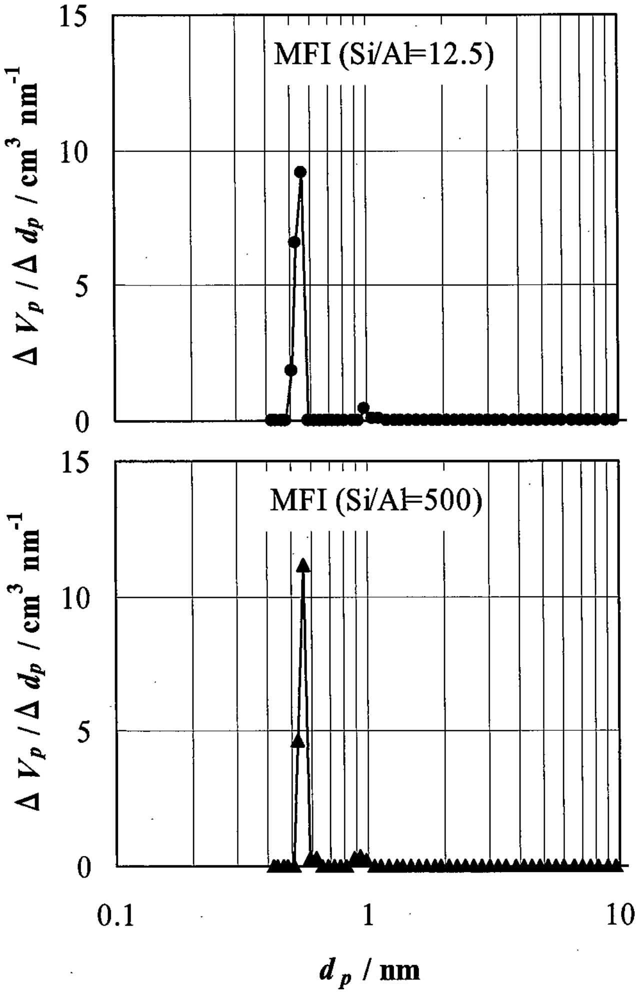

Figure 5-3. Pore size distributions for MFI zeolites (GCMC, BELSim).

the second small peak is detected at d_p=10 nm, whose peak is due to the step in N_2 isotherm (ca. p/p_0=0.1) (*cf.* Figure 5-5(a)). Accordingly, it is reasonable to conclude that the main peak at d_p=0.56 nm is due to MFI channel pores, and the second peaks at d_p=1 or 10 nm is not related to the pores of MFI channels, but to the ghost peak.

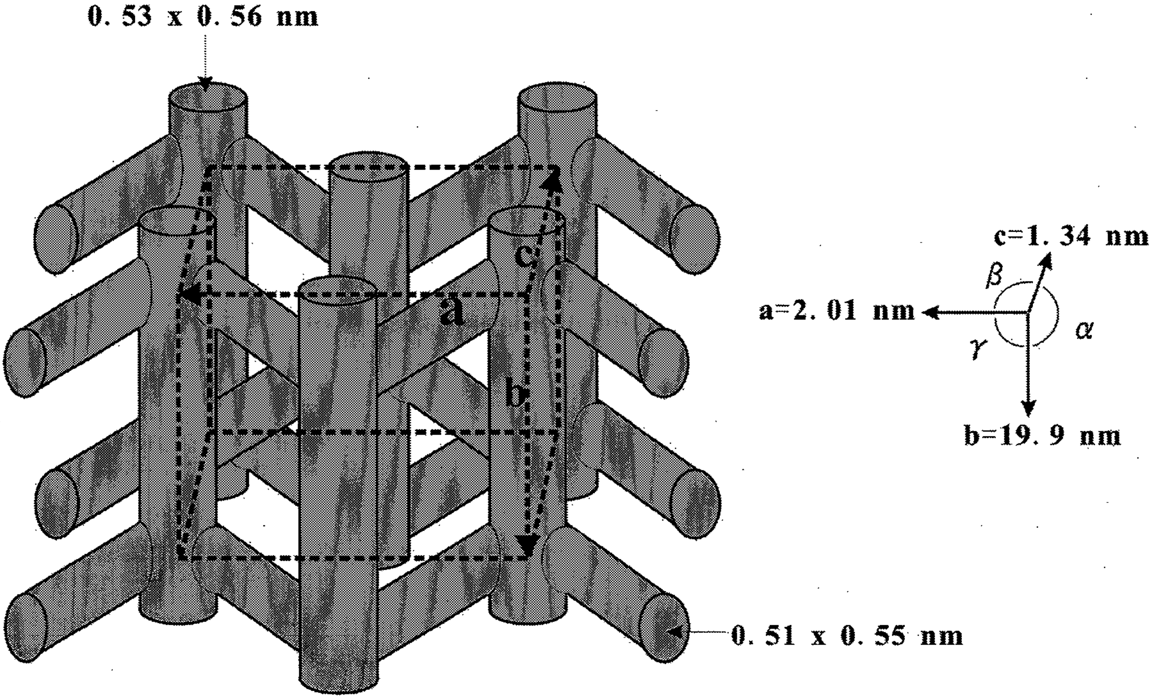

Figure 5-4. Channel structure of MFI zeolites.

5.3.2 Comparison of high resolution isotherms of N_2 and Ar for microporous MFI zeolite (Si/Al=500)

It is significant to compare the high resolution isotherms of N_2 and Ar for MFI zeolite, because, as was pointed before, N_2 is specific adsorptive and Ar nonspecific one. Figure 5-5(a) shows the high resolution adsorption isotherms of N_2 and Ar in the range of a_s=0.01–1.1 for the MFI zeolite (Si/Al=500) at their boiling points. Below a_s=0.6, as was seen from Figure 5(a), the N_2 isotherm is shifted to low relative pressure in comparison with the Ar isotherm, whose result suggests that interaction of N_2 with channel surface of MFI zeolite (Si/Al=500) is larger than that of Ar. Their adsorption energies will be given in the next section.

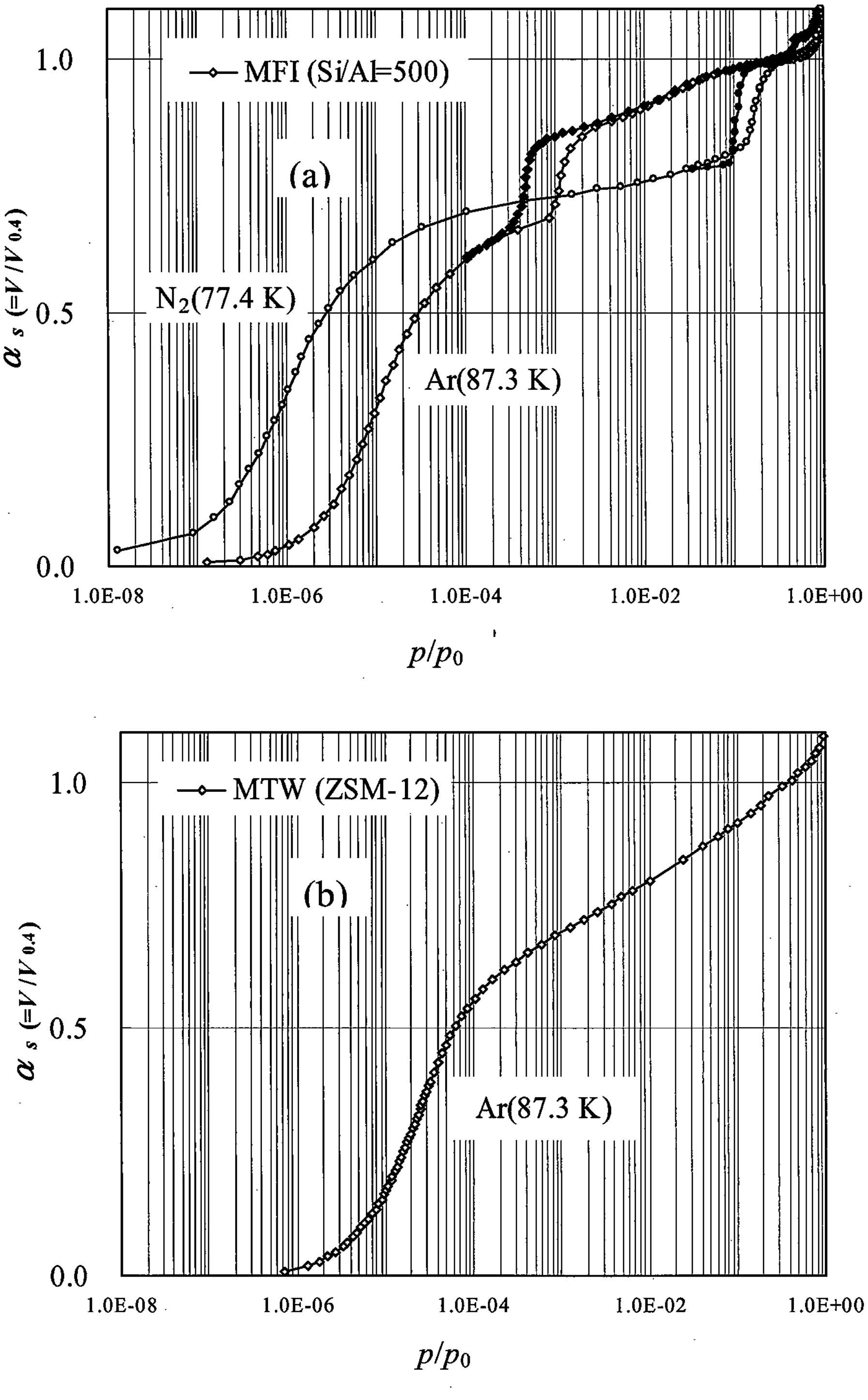

Figure 5-5. High resolution adsorption isotherms for zeolites ; (a) Ar and N_2 isotherms for MFI (b) Ar isotherm for MTW.

In both isotherms, the hystereses are detected; namely, the N_2 isotherm has hysteresis at p/p_0=0.1–0.2, while the Ar isotherm has hysteresis at $p/p_0=3\text{x}10^{-4}$–$2\text{x}10^{-3}$. The hysteresis of the N_2 isotherm for the present MFI zeolite (Si content = 99.6 mole%) is almost same as that reported by Muller and Unger [5] for Silicalite (Si content : 100 %). There is a large difference in the relative pressure of hysteresis between N_2 and Ar isotherms, but it is difficult to explain this difference in the present stage.

It is interesting to examine whether other zeolites give the hystereses (steps) shown in Figure 5-5(a). It was found that several zeolites (MTW, AFI, VFI, LTA, FAU) give no step in the high resolution Ar isotherms at the vicinity of $p/p_0=10^{-3}$ [6]. For example, the Ar isotherm for the MTW zeolite (ZSM-12) is shown in Figure 5-5(b). It is speculated that the hystereses detected in the N_2 and Ar isotherms are related to the channel structure of MFI zeolite, which consists of straight channels (channel size : 5.3 x 5.6 (Å)) and zigzag channels (channel size : 5.1 x 5.5 (Å)) (*cf.* Figure 5-4).

5.3.3 Comparison of differential adsorption energy of N_2 and Ar for microporous MFI zeolite (Si/Al=500)

In the previous section, it is suggested that interaction of N_2 molecules with channel surface of MFI zeolite (Si/Al=500) is greater than that of Ar atoms. In this section, the differential adsorption energies of N_2 and Ar are calculated on the basis of the high resolution

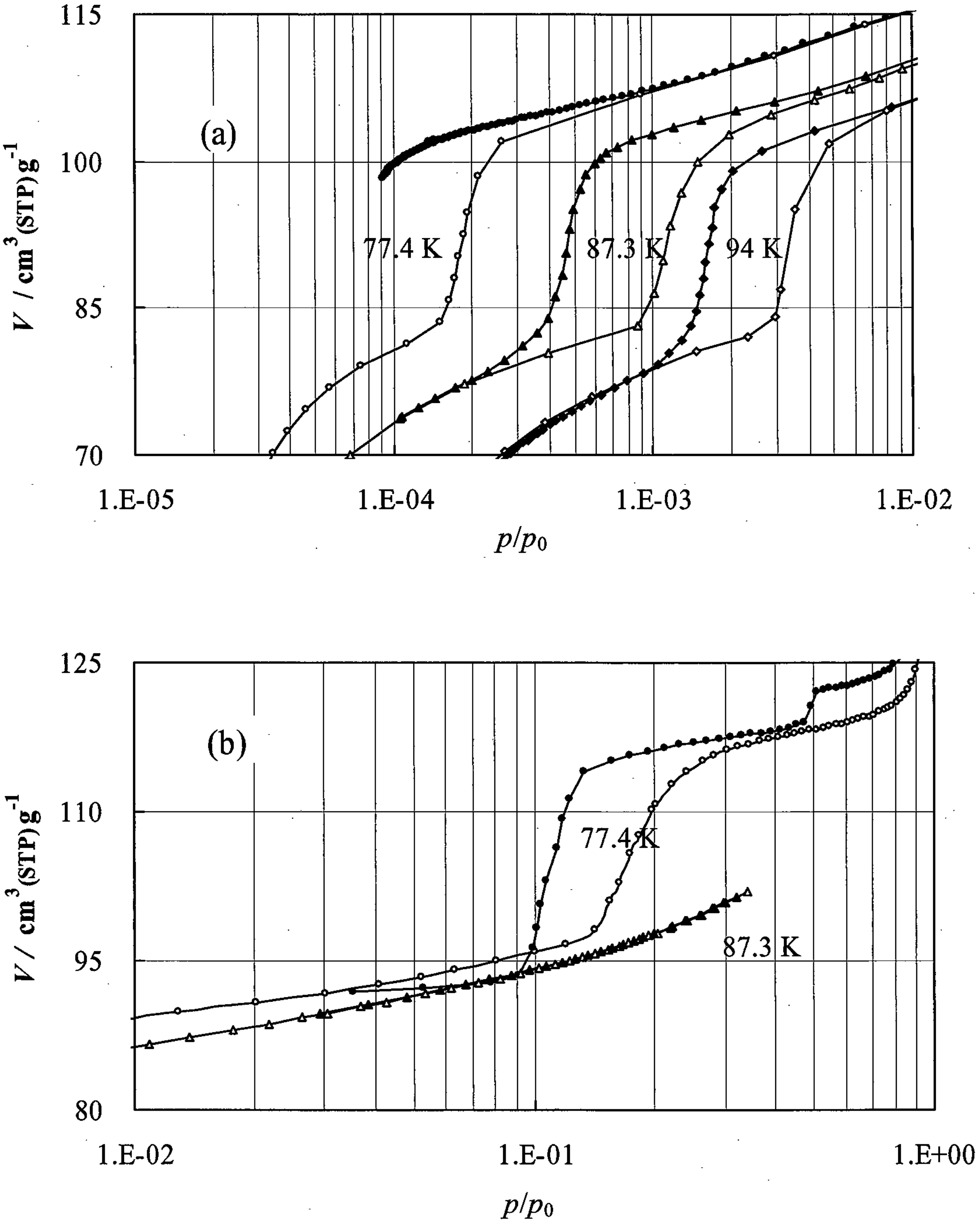

Figure 5-6. High resolution adsorption-desorption isotherms for MFI zeolite (Si/Al=500) ; (a) Ar isotherms (b) N_2 isotherms.

isotherms of both adsorbates. The Ar isotherms at 77.4 K, 87.3 K, and 94 K are shown in Figure 5-6(a), while the N_2 isotherms at 77.4 and 87.3 K are shown in Figure 5-6(b). In the N_2 isotherm at 77.4 K, there appear two hystereses; one above p/p_0=0.45, which may be attributed to capillary condensation, and the other at p/p_0=0.1 – 0.3, which may be attributed to the change of packing density of N_2 molecules trapped in the channel of MFI zeolite [3]. This phenomenon, however, has not been clarified yet. In Figure 5-7, the differential adsorption enthalpies ($\Delta\bar{h}_{ad}$) of N_2 and Ar are given as a function of a_s. At first, the adsorption energy at low filling, where the lateral interaction of adsorbates trapped in microporous channels of MFI is assumed to be small is discussed. As was shown in Figure 5-7, the differential adsorption energies for N_2 and Ar at a_s=0.1 are 10.0 kJ/mol and 5.0 kJ/mol, respectively. This experimental fact clearly indicates that the vertical interaction energy of the N_2 molecules with the channel surface of MFI zeolite is twice of that of the Ar atoms. Such difference in interaction energy may be due to the difference in character of two adsorptives; that is, N_2 is specific adsorptive with quadrupole, while Ar is nonspecific adsorptive (noble gas).

Next, the lateral interaction of the two adsorbates will be considered. In case of Ar (*cf.* Figure 5-7), its differential adsorption energy increases from 5.0 kJ/mol (a_s=0.1) to 17.4 kJ/mol (a_s=0.7), reaches maximum 17.4 kJ/mol (a_s=0.7–0.8), and then decreases to condensation energy 6.52 kJ/mol (87.3 K). On the other hand, in case of N_2, its

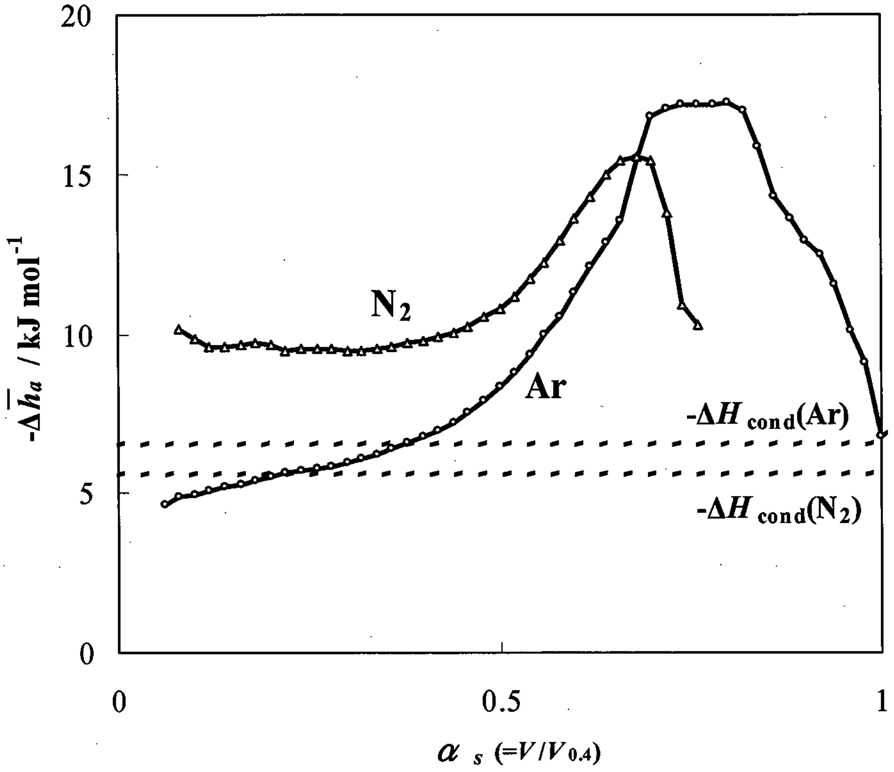

Figure 5-7. Differential adsorption enthalpies for MFI zeolite (Si/Al=500).

differential adsorption energy increases from 10.0 kJ/mol ($a_s=0.1$) to 15.4 kJ/mol ($\alpha_s=0.6_7$), reaches maximum 15.4 kJ/mol ($a_s=0.6_7$–0.7), and then decreases. From difference in the adsorption energies at $a_s=0.1$ and $a_s=0.7$, it is inferred that the lateral interaction of Ar atoms in the micropore channels of MFI zeolite is greater than that of N_2 molecules. This result is in sharp contrast to the vertical interaction mentioned above.

As was mentioned above, there is a large difference in hysteresis pressure between N_2 isotherm and Ar isotherm (*cf.* Figure 5-5(a)). It was tried to find the relation between difference in hysteresis pressure and difference in adsorption energies (vertical and lateral interactions), but it was unable to find the relation.

Finally, the phase transition of MFI zeolite crystal (ZSM-5) will be mentioned in connection with the hysteresis detected in the adsorption isotherm. It is known that the monoclinic-orthorhombic phase transition of MFI zeolites occurs at temperatures of 330–360 K, depending on Al content of MFI zeolite [7]. Takaishi and Tsutsumi [8] have pointed out that the hysteresis of *p*-xylene in its adsorption isotherm (352 K) is related to phase transition of ZSM-5 zeolite crystal. There is the large difference in temperature between the ZSM-5–*p*-xylene system (352 K) and the present adsorption system (77 K – 94 K). It is very important to investigate whether the phase transition of MFI zeolite crystal is brought about by the adsorption of N_2 or Ar.

5.4 Conclusion

The number of silanol groups has little influence on the Ar isotherm, but give an appreciable effect on the N_2 isotherms below a_s=0.5. Also, the proton content in zeolite channels has little influence on the Ar isotherm, but the significant effect was observed in the N_2 isotherms. Therefore, the Ar isotherms should be used in evaluation of microporosity of various zeolites having different channel or cage size.

Both Ar isotherm at 87.3K and N2 isotherm at 77.4K for MFI zeolite showed hysteresis. It is not the one for mesopore which can be seen in Type IV isotherm. It is speculated that the reason of the hysteresis may be because of the monoclinic-orthorhombic phase transition of MFI zeolites.

5.5 References

[1] S. J. Gregg, K. S. W. Sing, "*Adsorption, Surface Area and Porosity*", Academic Press, London, 1982.

[2] B. F. Mentzen, , J.-M. Letoffe, P. Claudy, *Thermochimica Acta*, **288**, 1 (1996).

[3] U. Muller, K. K. Unger, *Stud. Surf. Sci. Catal.*, **39**, 101 (1988).

[4] K. Nakai, M. Hakuman, H. Naono, *Abst. The 4th Pacific Basin Conference on Adsorption Science and Technology*, A6 (2006).

[5] K. Nakai, M. Hakuman, H. Naono, *Abst. International Symposium on Zeolites and Microporous Crystals*, p. 2046 (2006).

[6] K. Nakai, J. Sonoda, M. Yoshida, M. Hakuman, H. Naono, *Stud. Surf. Sci. Catal.*, **170A**, 831 (2007)

[7] H. Naono, M. Hakuman, T. Tanaka, N. Tamura, K. Nakai, *J. Colloid Interface Sci.,* **225**, 411 (2000).

[8] T. Takaishi, K. Tsutsumi, "*Catal. Lett.*, **13**, 97 (1996).

Chapter 6

Hydrophobic Modification of Ti-containing Zeolite (TS-1) and Their Applications in the Liquid-phase Selective Catalytic Reaction

6.1 Introduction

For many years, tetrahedrally coordinated transition metal oxides (e.g. Ti-, Cr-, Mo-oxide) containing porous materials such as zeolites and mesoporous silicas have attracted considerable attentions because of their unique catalytic and photocatalytic activities [1-19]. Especially, tetrahedral Ti-oxide species exhibited excellent catalytic properties in selective oxidation processes, i.e. phenol to cathecol and hydroquinone as well as olefins to epoxides, using alkyl hydroperoxide and hydrogen peroxide (H_2O_2) [3, 4, 10-19]. Ammoximation also proceeded over tetrahedral Ti-oxide species with ammonia and H_2O_2. Cyclohexanone was efficiently transformed to cyclohexanone oxime as a precursor of ε-caprolactam, which was important for production of nylon-6 [18, 19]. These systems were also environmentally friendly and promising in reducing the undesired byproducts.

On the other hand, it is well known that both of reaction rates and adsorption properties of reactants strongly depended on the surface hydrophilic-hydrophobic properties of catalysts and catalyst supports [9],[20]. The large number of surface hydroxyl groups showed affinity of water molecules, restricting the adsorption of reactants from air and aqueous solutions. Thus, in order to improve the adsorption properties of them, hydrophobically modified zeolites and mesoporous silicas were prepared in fluoride media using HF as well as fluorine containing structure-directing agent [9, 11]. The surface hydrophobic modification has also been attempted using silylation reagent [21-24]. It has been reported that the enhancement of photocatalytic activities for decomposition of organic pollutants was successfully attained by simple modification using triethoxyfluorosilane (TEFS) as silylation reagent, which have a stable ≡Si–F bond and reduced the affinity of water molecules [23, 24].

In the present work, aiming at the development of more efficient catalytic reaction systems using Ti-containing porous materials, hydrophobically modified Ti-containing zeolite (TS-1) was prepared by using TEFS (Scheme 6-1). The effect of surface modification on their catalytic activities for the liquid-phase ammoximation of cyclohexanone was also investigated.

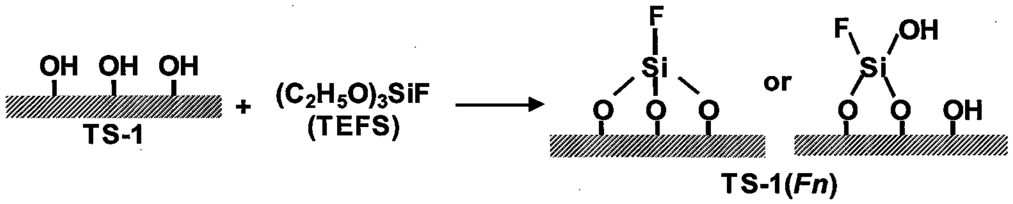

Scheme 6-1. Reaction scheme for surface modification by TEF.

6.2 Experimental

6.2.1 Preparation of TS-1

Ti-containing zeolite (TS-1, Si/Ti=58) was synthesized by direct hydrothermal synthesis method using tetraethyl orthosilicate, titanium isopropoxide and Tetrapropylammoniumhydroxide as template[17]. The mixture was transferred to a Teflon vessel autoclave and heated at 448 K for 24 h. After cooling to room temperature, the product was separated by centrifugiation, washed several times with ion exchanged water, dried at 373 K for 12h, and then calcined at 773 K for 5 h in air.

6.2.2 Hydrophobic modification

The surface modification of TS-1 was performed by grafting of TEFS onto TS-1 and expected to proceed as shown in Scheme 1.[23],[24] The mixture of TS-1 and 2-propanol solution of TEFS was stirred at 298 K for 5 h. Next, the sample was filtrated under vaccum, dried at 383 K for 12 h, and then calcined at 773 K for 5 h in air. TS-1 after grafting of TEFS were denoted as TS-1(*Fn*), where *n* described the TEFS contents in 2-propanol (*n* = 1, 5 wt.%).

6.2.3 Measurements

Prepared samples were characterized by XRD, UV-vis, photoluminescence as well as nitrogen and water adsorption-desorption measurements. XRD measurements were performed using a Rigaku RINT 2500 diffractometer with Cu Kα radiation (λ =1.5406 Å). UV-vis and photoluminescence spectrum were measured at 298 K with a Shimadzu UV-2450A double-beam digital spectrophotometer and a Spex Fluorog-3 spectrophotometer, respectively. Prior to the spectroscopic measurements, the samples were calcined in O_2 (>2.66 kPa) at 723 K for 1 h and then degassed at 473 K for 1 h.

6.2.4 Catalytic reaction

The ammoximation of cyclohexanone was used as the test reaction. Catalyst (50 mg), cyclohexanone (2 mmol), H_2O (5 ml), 30 % H_2O_2 (0.5 ml), 25 % aqueous solution of NH_3 (0.5 ml) and *tert*-butanol (5 ml) were charged into the reaction vessel and then heated at 353 K with stirring. The analysis of reaction product was performed on a gas chromatograph (Shimadzu GC-14B with FID detector) equipped with TC-1 capillary column.

6.3 Results and discussion

TS-1 showed the typical X-ray diffraction peaks attributed to the MFI structure (Figure 6-1(a)).[25] The diffraction peaks assigned to the MFI structure were clearly observed and their intensities were scarcely changed even after surface modification by TEFS (Figure. 6-1(b,c)).

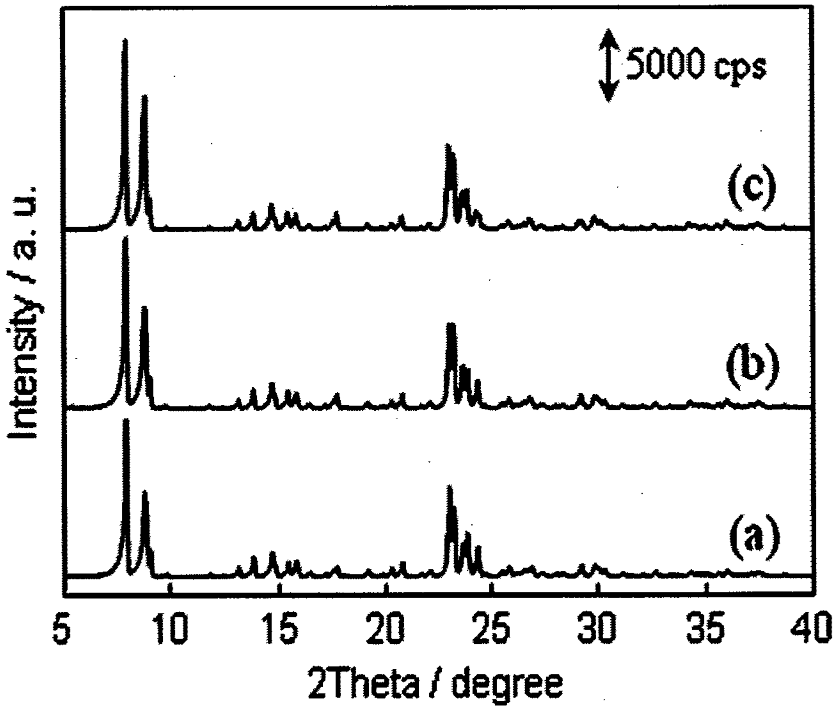

Figure 6-1. XRD patterns of (a) TS-1, (b) TS-1(*F1*) and (c) TS-1(*F5*).

The local structure of Ti-oxide species incorporated within the zeolite frameworks was also investigated by UV-vis and photoluminescence measurements. As shown in Figure 6-2(A), the appearance of distinct peak at around 220 nm can be assigned to the ligand to metal charge transfer

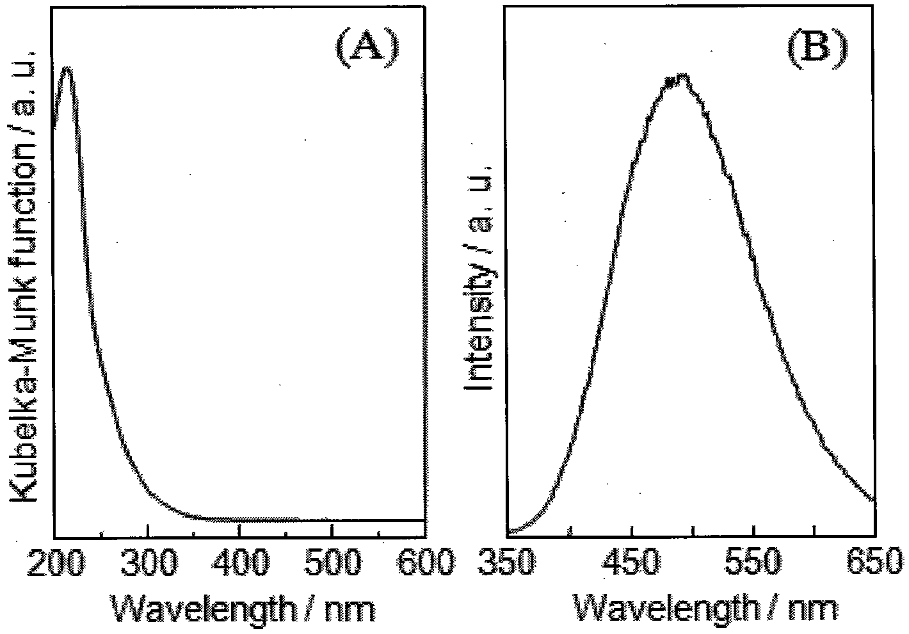

Figure 6-2. UV-vis (A) and photoluminescence spectrum (B) of TS-1(*F1*) measured at 298 K.

(LMCT) transition of tetrahedrally coordinated

Ti(IV)-oxide.[26, 27] Moreover, it was found that the almost same absorption spectra were observed before and after grafting of TEFS, suggesting that the local structure of Ti-oxide species were hardly affected by this surface modification treatment (data not shown).

Figure 6-2(B) shows the photoluminescence spectrum of TS-1(*F1*), which was observed in the wavelength region from 400 to 600 nm upon excitation of its LMCT band at around 220 nm at 298 K.

This photoluminescence can be attributed to the radiative decay process from charge transfer excited triplet state of tetrahedrally coordinated Ti(IV)-oxide to its ground state (eq. (1)) [9, 26, 27]. These results clearly indicated the presence of tetrahedrally coordinated Ti(IV)-oxide as the dominant species within TS-1(*F1*).

$$(\mathrm{Ti}^{4+}\text{–}\mathrm{O}^{2-}) \underset{hv'}{\overset{hv}{\rightleftarrows}} (\mathrm{Ti}^{3+}\text{–}\mathrm{O}^{-})^{*} \qquad (1)$$

Table 6-1. Characteristics of TS-1 and hydro-phobically modified TS-1

	TEFS content / wt.%	S_{BET} / $\mathrm{m^2 \cdot g^{-1}}$	Relative percentage of S_{BET} [a] / %	Water adsorption capacity [b] / $\mathrm{\mu mol \cdot m^{-2}}$
TS-1	0	434	100	3.65
TS-1(*F1*)	1.0	415	96	3.34
TS-1(*F5*)	5.0	362	83	1.00

[a] Relative percentages to BET surface area of unmodified TS-1

[b] Calculated by division of water adsorption capacity at $p/p_0 = 0.5$ by the value of S_{BET}

The information about the nitrogen adsorption-desorption behavior on modified and unmodified TS-1 was summarized in Table 6-1. The typical type I isotherms were observed in each sample. The BET surface area (S_{BET}) of samples were slightly decreased with an increase in the grafted amount of TEFS, however, TS-1(*F1*) and TS-1(*F5*) maintained large surface areas compared with original TS-1. The effect of the grafting of TEFS on the surface hydrophilic-hydrophobic properties of TS-1 was investigated by water adsorption measurement. As shown in Figure 6-3 and Table 6-1,

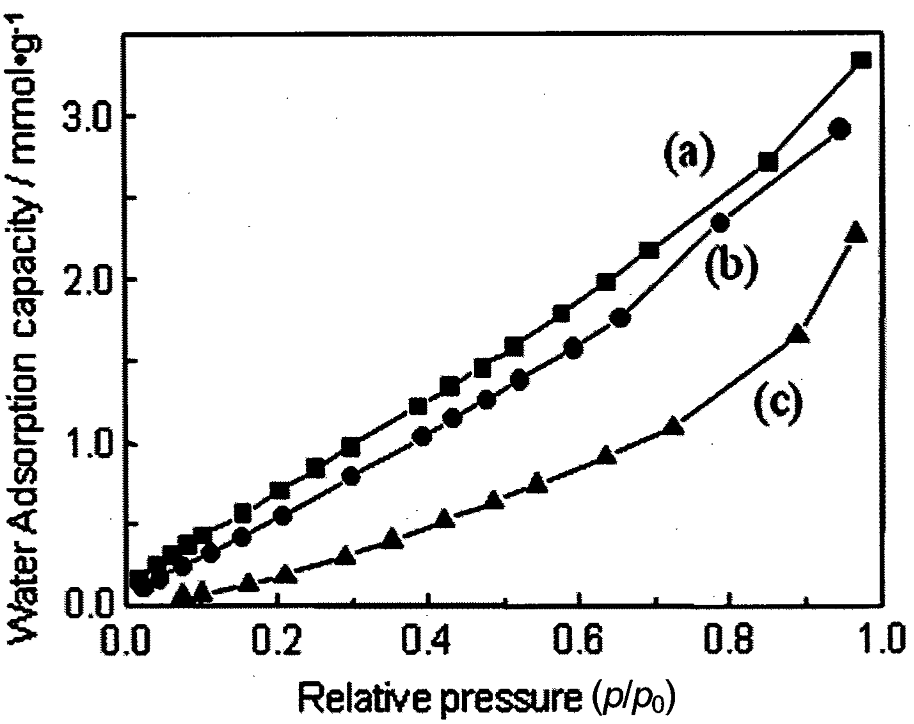

Figure 6-3. Water adsorption isotherms of (a) TS-1, (b) TS-1(*F1*) and (c) TS-1(*F5*) measured at 298 K.

water adsorption capacity of TS-1 was gradually decreased with an increase in the grafted amount of TEFS. The differences in the amount of adsorbed water can be ascribable to the different concentrations of surface hydroxyl groups in each sample. The presence of fluorine moieties on the surface of

TS-1(*Fn*) might also play significant roles for reducing the adsorbed amounts of water since the fluorine moieties tend to prevent the adsorption of water on the surface of TS-1.

XPS investigations also revealed the presence of fluorine moieties on the surface of TS-1(*Fn*). F_{1s} XPS peak was observed at around 689 eV, while no peak was detected in the case of original TS-1. This F_{1s} XPS peak was assigned to the covalent F atoms [28], which was different from the F^- ions on silica surface detected at around 685 eV [28], suggesting the formation of fluorine moieties through the reaction as shown in Scheme 1.

It could be seen that the surface hydrophobic modification of TS-1 leading to the decrease in the adsorbed amount of water was successfully attained through the removal of surface hydroxyl groups and anchoring of fluorine moieties by grafting of TEFS.

The liquid phase ammoximation of cyclohexanone was performed as the test reaction for investigating the effects of the surface hydrophobic modification of TS-1 on their catalytic activities. Figure 6-4 showed the turnover number (TON) defined as the ratio of produced cyclohexanone oxime to the amount of Ti-oxide species included in the catalyst. The selectivity of cyclohexanone oxime was as high as 99 %. The enhancement of catalytic activity was observed for TS-1(*F1*), which showed the less hydrophilicity compared with unmodified TS-1. Meanwhile, the catalytic activity of TS-1(*F5*) was lower than that on unmodified TS-1, although the hydrophobicity of TS-1(*F5*) was the highest among prepared catalysts. These results suggested that the catalytically active Ti-oxide species within

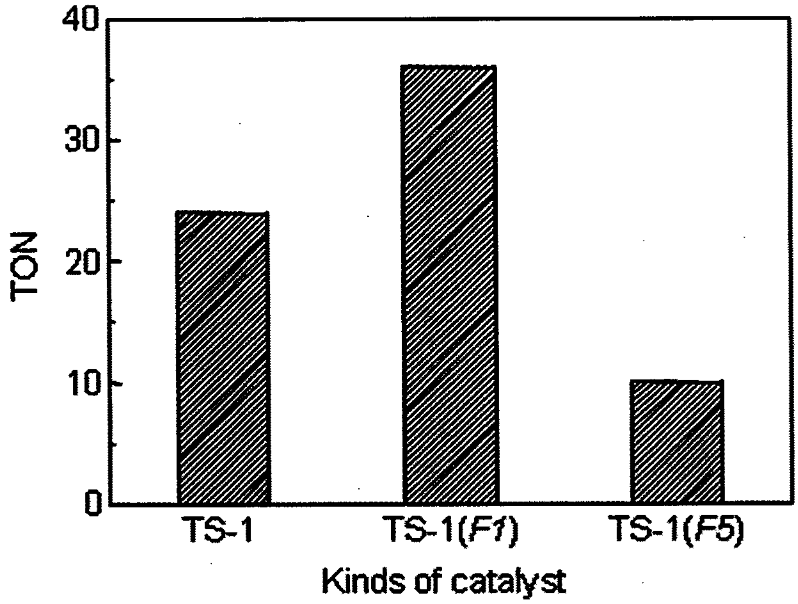

Figure 6-4. The turnover number (TON) for ammoximation of cyclohexanone to cyclohexanone oxime on each catalyst at 353 K. Reaction time: 1h.

the zeolite framework was gradually covered by fluorine moieties with increase in the amount of TEFS grafting, which play crucial role for enhancement of surface hydrophobicity and may lead to inhibiting the adsorption of reactants on Ti-oxide species. Therefore, the surface modification with small amounts of TEFS was effective for enhancement of catalytic activities.

6.4 Conclusion

Hydrophobic Ti-containing zeolite (TS-1(*Fn*)), which exhibited less water adsorption capacity, were successfully prepared by a simple surface modification of TS-1 by using TEFS. The MFI structures, large surface areas as well as the local structure of Ti-oxide species were scarcely changed after surface treatment. The grafting of suitable amount of TEFS onto TS-1 effectively enhanced the liquid-phase ammoximation of cyclohexanone, showing the possibilities for application of this simple modification technique in other reaction systems.

6.5 References

[1] H. Yamashita, K. Mori, *Chem. Lett.*, **36**, 348 (2007).

[2] H. Yamashita, M. Anpo, *Curr. Opin. Solid State Mater. Sci.*, **7**, 471 (2003).

[3] B. Notari, *Catal. Today*, **18**, 163 (1993).

[4] J.M. Thomas, R. Raja, D.W. Lewis, *Angew. Chem. Int. Ed.*, **44**, 6456 (2008).

[5] H. Yamashita, K. Yoshizawa, M. Ariyuki, S. Higashimoto, M. Che, M. Anpo, Chem. Commun., 435 (2001).

[6] T. Kamegawa, J. Morishima, M. Matsuoka, J.M. Thomas, M. Anpo, *J. Phys. Chem. C*, **111**, 1076 (2007).

[7] T. Kamegawa, R. Takeuchi, M. Matusoka, M. Anpo, Catal. Today, 111, 248 (2006).

[8] S. Higashimoto, Y. Hu, R. Tsumura, K. Iino, M. Matsuoka, H. Yamashita, Y.G. Shul, M. Che, M. Anpo, *J. Catal.*, **235**, 272 (2005).

[9] K. Ikeue, H. Yamashita, M. Anpo, *J. Phys. Chem. B*, **105**, 8350 (2001)

[10] P. Wu, T. Tatsumi, *Catal. Surv. Asia*, **8**, 137 (2004).

[11] Y. Goa, P. Wu, T. Tatsumi, J. Phys. Chem. B, **108**, 4242 (2004).

[12] Y. Kubota, Y. Koyama, T. Yamada, S. Inagaki, T. Tatsumi, *Chem. Commun.*, 6224 (2008).

[13] K. Mori, Y. Kondo, S. Morimoto, H. Yamashita, *J. Phys. Chem. C*, **112**, 397 (2008).

[14] K. Mori, K. Sugihara, Y. Kondo, T. Takeuchi, S. Morimoto, H. Yamashita, *J. Phys. Chem. C*, **112**, 16478 (2008).

[15] T. Blasco, A. Corma, M.T. Navarro, J.P. Pariente, *J. Catal.*, **156**, 65 (1995).

[16] M.A. Camblor, A. Corma, J.P. Pariente, *Zeolite*, **13**, 82 (1993).

[17] M.G. Clerici, G. Bellussi, U. Romano, *J. Catal.*, 129, 159 (1991).

[18] F. Song, Y. Liu, H. Wu, M. He, P. Wu, T. Tatsumi, *J. Catal.*, **237**, 359 (2006).

[19] H. Ichihashi, H. Sato, *Appl. Catal. A: Gen.*, **221**, 359 (2001).

[20] H. Yamashita, K. Maekawa, H. Nakao, M. Anpo, *Appl. Surf. Sci.*, **237**, 393 (2004).

[21] T. Kasahara, K. Inumaru, S. Yamanaka, *Micropore. Mesopore. Mater.*, 76, 123 (2004).

[22] T. Kimura, M. Suzuki, M. Maeda, S. Tomura, *Micropore. Mesopore. Mater.*, *95*, 213 (2006).

[23] Y. Kuwahara, T. Kamegawa, K. Mori, H. Yamashita, *Chem. Commun.*, 4783 (2008).

[24] Y. Kuwahara, K. Maki, Y. Matsumura, T. Kamegawa, K. Mori, H. Yamashita, *J. Phys. Chem. C*, **113**, 1552 (2009).

[25] A. Thangaraj, R. Kumar, S.P.Mirajkar, P. Ratnasamy, *J. Catal.*, **130**, 1 (1991).

[26] L. Marchese, E. Gianotti, V. Dellarocca, T. Maschmeyer, F. Rey, S. Coluccia, J.M. Thomas, *Phys. Chem. Chem. Phys.*, **1**, 585 (1999).

[27] L Marchese, T. Maschmeyer, E. Gianotti, S. Coluccia, J.M. Thomas, *J. Phys. Chem. B*, **101**, 8836 (1997).

[28] Y.Q. Wang, P.M.A. Sherwood, *Chem. Mater.*, **16**, 5427 (2004).

Chapter 7

Degradation of Isobutanol Diluted in Water over Visible Light Sensitive Vanadium Doped TiO_2 Photocatalyst

7.1 Introduction

For many years, titanium dioxide (TiO_2) photocatalysts have been investigated with considerable attention because they can be applicable for the decomposition of undesired compounds in air as well as wastewater [1-8], solar energy conversion [9,10] and production of clean energy resources through the water splitting reaction [11],[12]. Especially, applications for environmental issues such as purification of wastewater using natural solar light are of vital interest to practical utilizations and challenging topics. In this context, the development of visible light sensitive TiO_2 was intensively studied since the pure TiO_2 only show fascinating photocatalytic activities under UV light, which limited the use of a small UV fraction of natural solar light (ca. 3 %). To create a bathochromic shift of band gap energy, a number of research groups have been tested the doping of transition metal cations such as V, Cr, Fe, and Ni into TiO_2 by various method such as sol-gel method and ion implantation [13],[14]. Asahi et al. also reported that visible light sensitive TiO_2 could be prepared by the doping of nitrogen atoms into TiO_2, which exhibited photocatalytic activities for the degradation of methylene blue and gaseous acetaldehyde [15].

On the other hand, it has been reported that surface hydrophilic-hydrophobic properties of catalysts and catalysts supports strongly affected the reaction rate and adsorption property of reactants [16-18]. The enhancement of the adsorption of organic compounds from aqueous solutions and gas phase on the surface of porous materials and TiO_2 was successfully attained by surface hydrophobic modifications using fluorine sources [7],[8],[18-20].

In the present study, the design of visible light sensitive TiO_2 photocatalyst through the doping of vanadium into TiO_2 under the sol-gel process as well as hydrothermal treatment and their application in the photocatalytic degradation of isobutanol diluted in water was studied. The influences of the preparation methods and the amounts of doping vanadium species into TiO_2 were examined in detail. Moreover, the effect of the addition of NH_4F on the surface property, crystallinity and photocatalytic activity was investigated by several physicochemical characterizations for the purpose of the development of multifunctional TiO_2 photocatalyst.

7.2 Experimental

7.2.1 Preparation of vanadium doped TiO_2 photocatalyst

Tetraisopropyl orthotitanate (TPOT: $Ti(OC_3H_7)_4$), vanadium acetylacetonate ($V(CH_3COCHCOCH_3)_3$), ethanol and NH_4F were commercial products. All chemicals were used as received. The starting solutions were prepared by the addition of aqueous solution of NH_4F to the mixed TPOT-$V(CH_3COCHCOCH_3)_3$-ethanol solutions (Scheme 1). The molar ratio of starting solutions were as follows; Ti : H_2O : C_2H_5OH : NH_4F : V = 1 : 5 : 5 : X : Y (X = 0, 0.05, Y = 0, 0.002, 0.01,

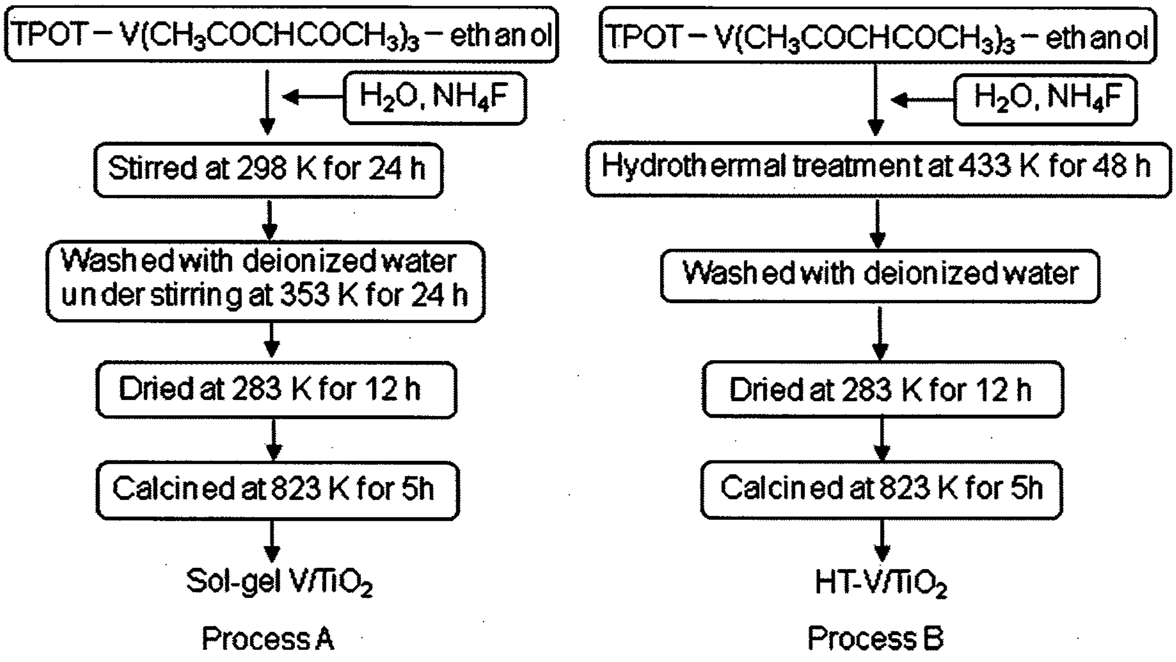

Scheme 1. Synthesis of Sol-gel V/TiO2 and HT-V/TiO_2

0.02). For preparation of V/TiO_2 by the sol-gel method, above starting mixture was stirred at 298 K for 24 h and then washing in water at 353 K for 24 h (Process A). The hydrothermal syntheses of V/TiO_2 in the absence and presence of NH_4F were performed using conventional autoclave (Process B). The starting mixture was transferred into an autoclave and kept at 433 K for 48 h. After centrifugation, washing and drying, both types of samples were calcined at 823 K for 5 h. Hereafter, vanadium doped samples prepared by the sol-gel and hydrothermal treatment in the presence of NH_4F were denoted as the sol-gel V/TiO_2(*n*) and HT-V/TiO_2(*n*), respectively, where *n* described the vanadium contents (%) of each sample.

7.2.2 Apparatus and procedures

UV-vis absorption spectra were recorded with Shimadzu UV-2450 spectrophotometer. X-ray diffraction of all samples was also measured by Rigaku RINT2500 diffractometer with Cu Kα radiation (λ = 1.5406 Å). The photocatalytic activity of samples was evaluated by the degradation of isobutanol diluted in water. The fixed amounts of catalysts (50 mg) were dispersed in 25 ml of isobutanol solution (2.61 mmol/L). After stirring under dark conditions for 30 min, the solution was bubbled by oxygen for another 30 min. Then, UV and visible light irradiation (λ > 430 nm) was carried out using 100 W high-pressure Hg lamp or 500 W Xe-lamp and colored filters (HOYA; L-43), respectively. The progress of the reactions was monitored by gas chromatography analysis (GC-14B, Shimadzu). Water adsorption isotherms of the catalysts were measured at 293 K using a conventional vacuum system.

7.3 Results and Discussion

7.3.1 Catalysts characterization

As shown in Fig. 7-1, sol-gel V/TiO_2 and HT-V/TiO_2 with different contents of vanadium after calcinations at 823 K only show peaks due to the presence of TiO_2 anatase phase, indicating that vanadium oxide species were highly dispersed within TiO_2 without the formation of large vanadium oxide clusters under the sol-gel and hydrothermal treatments. The intense diffraction peak assigned to the (101)

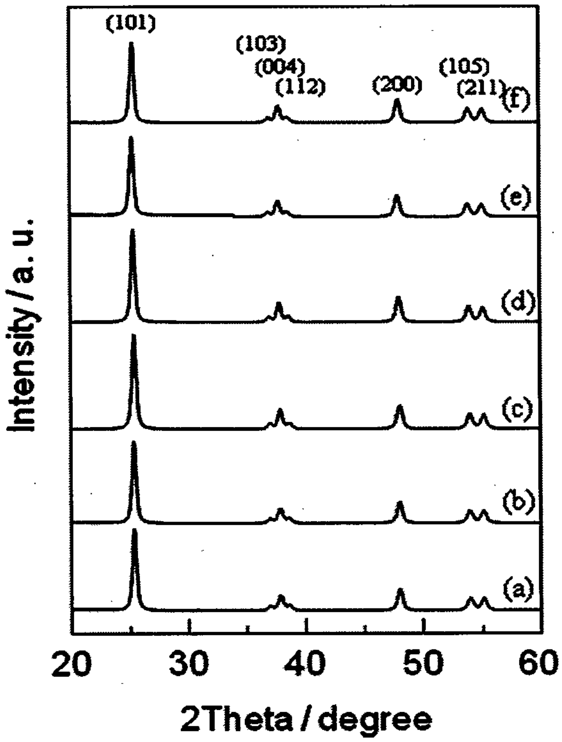

Figure 7-1. XRD patterns of (a) sol-gel TiO_2, (b) sol-gel $V/TiO_2(1.0)$, (c) HT-TiO_2 and (d-f) HT-$V/TiO_2(n)$ (n = (d) 0.2, (e) 1.0 and (f) 2.0).

reflection of TiO_2 anatase phase was slightly decreased with increasing of vanadium contents (Figure 7-1(c-f)). However, the peak intensity of HT-V/TiO_2 was higher than those of sol-gel TiO_2 and $V/TiO_2(1.0)$, showing that the synthesis of highly crystalline V/TiO_2 was successfully achieved by the hydrothermal treatment. It was also found that the BET surface area of sol-gel TiO_2 (36 m^2/g) was small as compared to those of HT-V/TiO_2. In the series of HT-V/TiO_2, BET surface areas were almost same values (ca. 50 m^2/g). The crystalline size of HT-V/TiO_2 was also calculated by applying the Scherrer's equation for

(101) reflection of TiO_2 anatase phase. The crystalline size could be determined to be about 20 nm in the series of HT-V/TiO_2, suggesting that the crystalline sizes were hardly affected by the contents of vanadium oxide species.

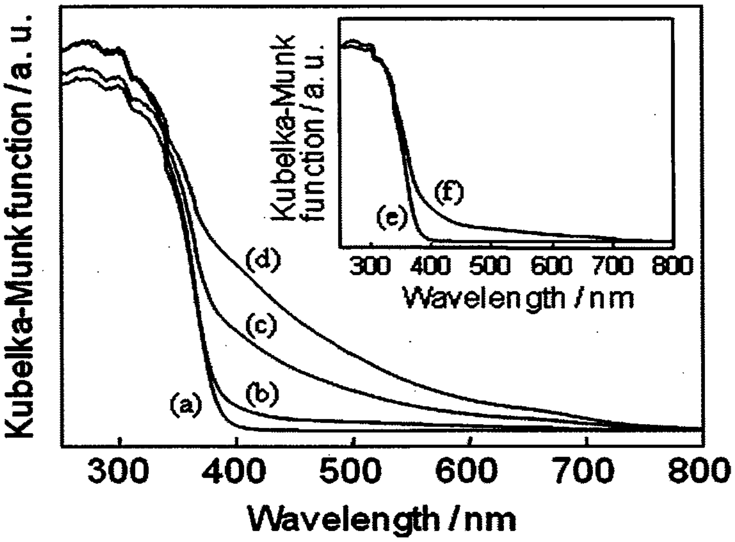

Figure 7-2. UV-vis spectra of pure TiO_2 and V/TiO_2 prepared by the sol-gel and hydrothermal treatments

Figure 7-2 shows UV-vis spectra of pure TiO_2 and V/TiO_2 prepared by the sol-gel and hydrothermal treatments. Pure TiO_2 (Figure 7-2(a,e)) exhibited the absorption edge at around 380 nm, which corresponded to the band gap of anatase type TiO_2. On the other hand, V/TiO_2 showed the long-tailed absorption in the visible light region above 380 nm as a shoulder peak. This visible light absorption due to the formation of the impurity energy levels within the band gap of TiO_2 was also increased with further increasing the vanadium contents from

0.0 to 2.0 % (Figure 7-2(a-d)). These results clearly indicated that the visible light sensitive TiO_2 possessing the high crystallinity of anatase phase was briefly prepared by controlling the doping amount of vanadium species into TiO_2.

7.3.2 Photocatalytic degradation of isobutanol over sol-gel V/TiO_2 and HT-V/TiO2

Based on the above characterizations, it was found that the crystalline V doped TiO_2 was successfully prepared by the sol-gel and hydrothermal treatment and can be expected to show photocatalytic activities even under visible light. Thus, the reaction rates for the photocatalytic degradation of isobutanol diluted in water were investigated over sol-gel V/TiO_2 and HT-V/TiO_2 with different contents of vanadium under visible light ($\lambda > 430$ nm).

As shown in Figure 7-3, the degradation of isobutanol proceeded on sol-gel V/TiO_2(1.0) and HT-V/TiO_2(0.2, 1.0 and 2.0), while pure TiO_2 (both of HT-TiO_2 and sol-gel TiO_2) did not show any photocatalytic activities under visible light ($\lambda > 430$ nm). In this reaction, isobutanol was finally decomposed into CO_2 and H_2O through the intermediate products such as ketone and aldehyde (data not shown). The reaction rate for the degradation of isobutanol strongly depended on the doping amount of vanadium, and among these, HT-V/TiO_2(1.0) exhibited the highest enhancement in the reaction rate. The reaction rate of HT-V/TiO_2(1.0) was about 2.4 times larger than that on sol-gel

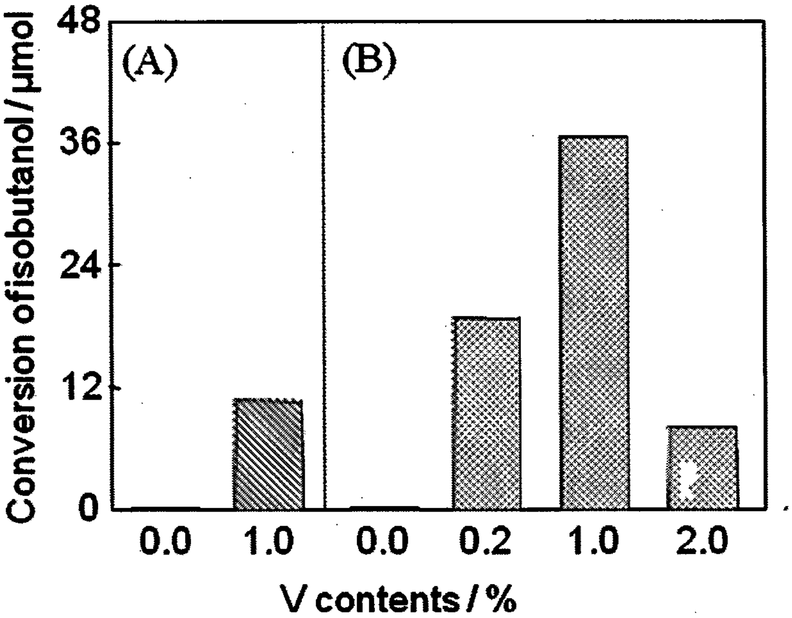

Figure 7-3. Photocatalytic degradation of isobutanol diluted in water over pure TiO_2 and V/TiO_2 with different contents of vanadium prepared by (A) sol-gel and (B) hydrothermal treatment in the presence of NH_4F under visible light (λ > 430 nm) irradiation. Reaction time: 24 h

$V/TiO_2(1.0)$. The higher crystallinity of the anatase phase as well as the larger surface area of HT-$V/TiO_2(1.0)$ plays crucial roles for enhancement in the reaction rate. Moreover, in the region of higher vanadium contents, impurity energy levels act as the recombination center of photo-formed electron and hole, leading to the decreasing of reaction rate [12]. These results clearly indicated that the reaction rate was effectively improved by the small amounts of vanadium doping into TiO_2.

The same reaction was also performed to confirm the effect of the vanadium doping into TiO_2 on the reaction rate for the degradation of isobutanol under UV light irradiation. As shown in Figure 7-4, hydrothermally synthesized samples showed higher reaction rate, and were scarcely affected by the doping of vanadium compared with sol-gel TiO_2. These results suggested that the successful preparation of

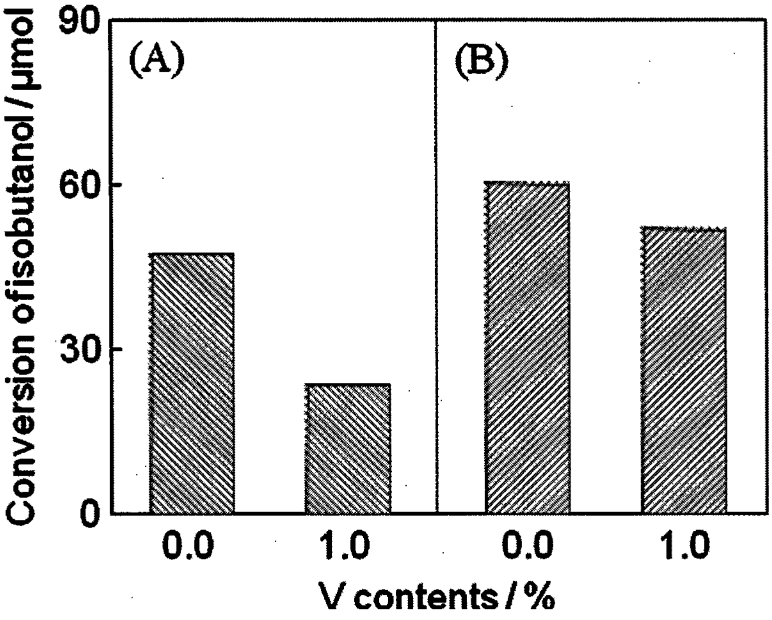

Figure 7-4. Photocatalytic degradation of isobutanol diluted in water over pure TiO_2 and $V/TiO_2(1.0)$ prepared by (A) sol-gel and (B) hydrothermal treatment in the presence of NH_4F under UV light irradiation. Reaction time: 1 h

visible light sensitive V/TiO_2 showing high photocatalytic activities not only under UV but also visible light were achieved by applying the hydrothermal treatment.

Finally, the degradation of aqueous isobutanol over two types of V/TiO_2(1.0) prepared by the hydrothermal treatment in the absence and presence of NH_4F (X = 0, 0.05) were also carried out under visible light irradiation (λ > 430 nm). The formation of highly crystalline TiO_2 was reported by the addition of fluorine sources into the starting solution of TiO_2 [20]. In fact, the comparative study revealed that V/TiO_2(1.0) prepared in the presence of NH_4F (HT-V/TiO_2(1.0)), which possessed high crystallnity of anatase phase, exhibited higher photocatalytic

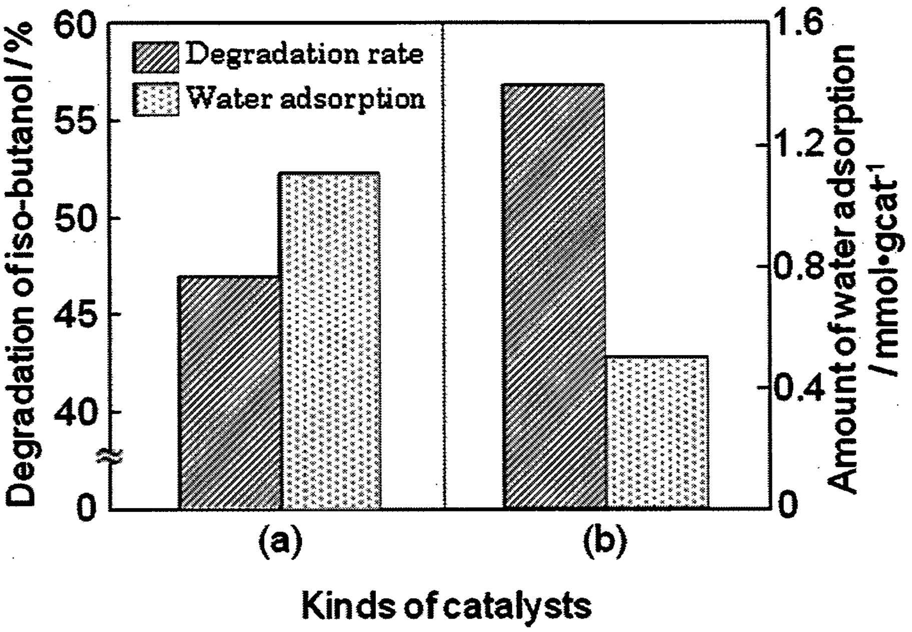

Figure 7-5. The photocatalytic activities for the degradation of isobutanol in water under visible light (λ > 430 nm) irradiation and the amount of water adsorption over V/TiO_2(1.0) prepared by hydrothermal treatment in the presence (a) and absence (b) of NH_4F. Reaction time: 24 h.

activity than that on V/TiO_2(1.0) prepared in the absence of NH_4F, as shown in Figure 7-5. Moreover, it was found that the amount of adsorbed water on HT-V/TiO_2(1.0) was much smaller than that on V/TiO_2(1.0) prepared in the absence of NH_4F. Therefore, less affinity of the H_2O molecules on the surface of HT-V/TiO_2(1.0) will enhance the transfer of organics from water to catalysis surface, which also led to the higher photocatalytic activities of HT-V/TiO_2(1.0).

7.4 Conclusion

In conclusion, vanadium doped TiO_2, which exhibited the photocatalytic activities not only under UV but also visible light, were successfully prepared by the hydrothermal treatment with high crystallinity and large surface area. The reaction rate for the degradation of isobutanol on HT-V/TiO_2(1.0) exhibited about 2.4 times larger than that on sol-gel V/TiO_2(1.0), showing that the high crystallinity of TiO_2 phase as well as the large surface area plays an important role in this reaction. Moreover, the hydrophobically modified HT-V/TiO_2(1.0), which was synthesized by the addition of NH_4F in the starting solutions, exhibited the higher photocatalytic activity as compared to that on V/TiO_2(1.0) prepared in the absence of NH_4F.

7.5 References

[1] M.R. Hoffmann, S.T. Martin, W.Y. Choi, D.W. Bahnemann, Chem. Rev., 95, 69 (1995)

[2] A. Fujishima, T.N. Rao, and D.A. Tryk, J. Photochem. Photobio. C: Photochem. Rev., 1, 1 (2000)

[3] H. Yamashita, Y. Ichihashi, M. Harada, G. Stewart, M.A. Fox, and M. Anpo, J. Catal., 158, 97 (1996).

[4] H. Kominami, H. kumamoto, Y. Kera, and B. Ohtani, J. Photochem. Photobio. A: Chem., 160, 99 (2003)

[5] H. Yamashita, Y. Nishida, S. Yuan, M. Narisawa, Y. Matsumura, T. Ohmichi, I. Katayama, Catal. Today, 120, 163 (2006)

[6] Y. Kuwahara, T. Kamegawa, K. Mori, and H. Yamashita, Chem. Commun., 4783 (2008)

[7] Y. Kuwahara, K. Maki, Y. Matsumura, T. Kamegawa, K. Mori, and H. Yamashita, J. Phys. Chem. C, 113, 1552 (2009)

[8] X. You, F. Chen and J. Zhang, J. Sol-Gel Sci.Technol., 34, 181 (2005)

[9] M. Grätzel, *J. Photochem. Photobio. A: Chem.*, **164**, 3 (2004)

[10] P.V. Kamat, *J. Phys. Chem. C*, **111**, 2834 (2007)

[11] A. Kudo, *Catal. Surv. Asia*, 7, 31 (2003).

[12] M. Matsuoka, M. Kitano, M. Takeuchi, K. Tsujimaru, M. Anpo, and J.M. Thomas, *Catal. Today*, **122**, 51 (2007)

[13] W. Choi, A. Termin, and M.R. Hoffmann, *J. Phys. Chem.*, **98**, 13669

(1994)

[14] H. Yamashita, M. Harada, J. Misaka, M. Takeuchi, B. Neppolian, M. Anpo, *Catal. Today* **84**, 191 (2003).

[15] R. Asahi, T. Morikawa, T. Ohwaki, K. Aoki, Y. Taga, *Science*, **293**, 269 (2001)

[16] H. Yamashita and K. Mori, *Chem. Lett.*, **36**, 348 (2007)

[17] H. Yamashita, K. Ikeue, T. Takewaki, and M. Anpo, *Top. Catal.*, **18**, 95 (2002).

[18] S. Yuan, S. Kawasaki, K. Mori, and H. Yamashita, *Res. Chem. Intermed.*, **34**, 331 (2008)

[19] Q. Yuan, R. Ravikrishna, and K.T. Valsaraj, *Sep. Purif. Technol.*, **24**, 309 (2001)

[20] T.K. Pong, J. Besida, T.A. O'Donnell, and D.G. Wood, *Ind. Eng. Chem. Res.*, **34**, 308 (1995)

[21] J. C. Yu, J. Yu, W. Ho, Z. Jiang, and L. Zhang, *Chem. Mater.*, **14**, 3808 (2002).

Chapter 8

Summary and General Conclusion

8.1 Purpose of this study

A new volumetric adsorption measuring system which can measure accurate low pressure adsorption isotherms was developed. The pore structure of zeolite was studied by gas adsorption technique using the system. Also, the hydrophobic properties of catalysts surface were examined by water vapor adsorption measurement.

8.2 Summary

8.2.1 Summary of Chapter 2

A new volumetric gas adsorption apparatus into which the dead volume measurement cell (dVd cell) is incorporated. The dVd cell measures continuously the change of dead volume during adsorption measurement. The dead volume at every step of adsorption measurement is used in calculation of adsorbed amount of nitrogen gas. Introduction of the dVd cell makes the level-control system of liquid nitrogen unnecessary, and reduces the adsorption amount error due to the minute fluctuation of liquid–nitrogen level. The sensitivity and reproducibility of the new adsorption apparatus developed in this sudy have been examined using some certified materials.

Adopting the new volumetiric adsorption theory, a high-accurate adsorption system was developed for measuring low pressure isotherm.

8.2.2 Summary of Chapter 3

A new volumetric adsorption apparatus, BELSORP-max™ was developed to measure adsorption isotherms from relative pressure as low as 1x10^{-9} (N_2 at 77K, Ar at 87K).

The high resolution adsorption isotherm of N_2 at 77K from extremely low relative pressure to non-porous and microporous carbon materials were measured by BELSORP-max™. Two kinds of nonporous carbon whose name was carbon blacks, (#51) and graphitised carbon black (LGC2102) were utilized to get a new standard a_s-data and t-data from the very low relative pressure. On the other side, an activated carbon was used as represented microporous carbon materials (MPAC: AX-21) to know adsorbed amounts from the low-pressure region, which there could not have ever been for technical difficulties like high ultimate vacuum achievement. In other words, the new technique provides more rigorous pore size distributions (PSD) and pore volumes (PV). Besides the examination of the adsorbed amount of MPAC, PSD and PV were also investigated from HK and BJH of classical calculation for PSD as well as a molecular simulation of NLDFT (BELSim™). When the adsorption isotherm of MPAC from the $p/p_0=10^{-6}$ and that from $p/p_0=10^{-9}$ was compared, the details of the hided adsorbed amount about 60cm^3(STP)/g from 10^{-9} to 10^{-6} were clearly found. Accordingly, the differences have possibility around 0.5% PSD measurement error.

8.2.3 Summary of Chapter 4

Ar isotherms (87.3 K) and N_2 isotherms (77.4 K) were measured for two silicas with different silanol content and two MFI zeolites with different alumina (proton) content. Silanols or protons give the significant effect on N_2 isotherms, but little influence on Ar isotherms. Ar isotherms for seven zeolites of various micropore size were measured in the pressure range of $p/p_0=10^{-7}$–0.99. Zeolites used are MFI (ZSM-5), MTW (ZSM-12), AFI (SSZ-24), AFI (AlPO-5), VFI (VPI-5) [group A], and LTA (Type A-Ca), FAU (Type Y) [group B]. Group A zeolites have micropore channels without cage, while group B zeolites have the window and cage. It has been found that the Polanyi adsorption potential of Ar atoms for the group A zeolites is closely related with channel size, and the adsorption potential of the group B zeolites depends on both of cage size and channel size.

8.2.4 Summary of Chapter 5

The high resolution adsorption isotherms of N_2 (77.4 K) and Ar (87.3 K) have been measured for two nonporous silicas with different silanol contents (3.3 and 0.35 OH/nm^2) and for two MFI zeolite with different Al contents (Si/Al=12.5 and 500). Silanol groups and Al sites (acid sites) give the significant effect on the N_2 isotherms at submonolayer, but the Ar isotherms are independent of silanols and Al sites. The Ar isotherms, therefore, are preferable in calculation of microporosity of zeolites. The N_2 and Ar isotherms for MFI zeolite

(Si/Al=500) have been measured at temperatures of 77 – 94 K, from which the differential adsorption energies of N_2 and Ar are calculated. The interaction of N_2 with channel surface of MFI zeolite is greater than that of Ar in the range of a_s=0.1 – 0.7. The hystereses are detected for the N_2 isotherm in p/p_0=0.1–0.3 at 77.4 K and for the Ar isotherm in $p/p_0=3\text{x}10^{-4}–2\text{x}10^{-3}$ at 87.3 K. However, it is difficult to explain the hysteresis phenomenon using differential adsorption energy.

8.2.5 Summary of Chapter 6

Hydrophobic modification of Ti-containing zeolite (TS-1) was performed by using triethoxyfluorosilane (TEFS). TS-1 after modification with TEFS (1 wt%) showed higher catalytic activity for the ammoximation of cyclohexanone than those on unmodified and modified TS-1 with TEFS (5 wt.%) due to the effective modification without covering of underlying catalytically active Ti-oxide species.

8.2.6 Summary of Chapter 7

Vanadium doped and non-doped TiO_2 photocatalysts (V/TiO_2 and pure TiO_2) were prepared by sol-gel and hydrothermal synthesis method in the presence and absence of NH_4F. V/TiO_2 exhibited the long-tailed absorption in the visible light region above 380 nm, however, pure TiO_2 only shows the absorption in the UV light region. Degradation of isobutanol diluted in water proceeded efficiently on

V/TiO_2 even under visible light ($\lambda > 430$ nm), which corresponded to the light absorption of prepared samples. Moreover, it was found that the hydrothermally synthesized V/TiO_2 in the presence of NH_4F showed higher photocatalytic activities than those on V/TiO_2 prepared by the sol-gel and hydrothermal treatment in the absence of NH_4F, which was attributed to the high crystallinity of anatase phase and hydrophobic surface of V/TiO_2 prepared in the presence of NH_4F.

8.3 General Conclusion

Summarizing the results of each chapter, the following conclusions can be drawn.

[1] A new method to correct for the influence of liquid nitrogen level change was invented. It can eliminate other potential sources of the dead volume error, such as the fluctuation of the ambient temperature and liquid nitrogen temperature and change in atmospheric pressure as well. As a result, the highly accurate and reproducible adsorption isotherms could be obtained. The method makes it possible to measure adsorption isotherm of low surface area material (e.g. $0.1 m^2$ in total surface area) without using krypton gas.

[2] Using the new volumetric adsorption technique, a high-accurate gas adsorption system was developed. In conventional gas adsorption

instruments, solenoid valves are used. Instead of the valve, pneumatic valves are used for the system to reduce the gas emission from the seat material. The high resolution adsorption isotherm of N_2 at 77K from extremely low relative pressure ($p/p_0=10^{-9}\sim$) could be measured. Its performance is useful for the evaluation of the microporous material such as zeolite and activated carbon.

[3] From the high resolution adsorption isotherms of N_2 (at 77.4K) and Ar (at 87.3K), It was found that silanol groups and Al sites (acid sites) gives the significant effect on the N_2 isotherms at submonolayer, but the Ar isotherms are independent of silanols and Al sites. Therefore, for pore size evaluation of zeolites, Ar is preferable.

[4] For some zeolites, the both N_2 and Ar adsorption isotherms show hystereses between their adsorption and desorption isotherms. It is suggested that the phenomenon are related to the channel structure of MFI zeolite, which consists of straight channels and zigzag channels and there is a possibility that the phase transition of the zeolite crystal may cause the phenomenon.

[5] Two series of fluorine-modified catalysts were synthesized. The hydrophobic properties of the catalysts surface were examined by using BELSORP-max and investigated the catalytic performances. By the fluorine-modification, the water adsorption was suppressed and the

catalytic reaction was improved. It was found that the fluorine-modification (hydrophobic pretreatment) is effective for improving the catalytic performance.

Acknowledgement

The author, Joji Sonoda, expresses his sincerest gratitude to his supervisor, Professor Hiromi Yamashita of the Division of Materials and Manufacturing Science, Graduate School of Engineering, Osaka University for his constructive guidance fruitful discussions and kind encouragement throughout his study. Sincere thanks are extended to Professor Toshihiro Tanaka and Professor Shinji Fujimoto of Osaka University for their critical reading of this thesis and their helpful comments for its improvement. He acknowledges the support of Associate Professor, Kosuke Mori, Assistant Professor, Takeshi Kamegawa and Technical Stuff, Tetsuro Ohmichi, for their instructive discussions, suggestions and continual encouragement through out this work.

The author wishes to thank Doctor Hiromitsu Naono, Doctor Kazuyuki Nakai and Doctor Masayuki Yoshida of BEL Japan, Inc., whose comments made enormous contribution to my work.

The author would like to express his gratitude to his parents and his family for their understanding and strong encouragement towards his research work.

December, 2009

Joji SONODA

List of Publications Related to This Thesis

1) H. Naono, J. Sonoda, K. Oka, M. Hakuman
"Evaluation of Microporous Texture of Undecomposed and Decomposed ß-FeOOH Fine Particles by Means of Adsorption Isotherms of Nitrogen Gas and Water Vapor"
Proceedings of the IV International Conference on Fundamentals of Adsorption, pp. 17-22 (1992).

2) K. Nakai, J. Sonoda, S. Kondo, I. Abe
"The Analysis of Surface and Pores of Activated Carbons by the Adsorption of Various Gases"
Pure and Applied Chemistry, **65**, 2181 (1993).

3) 仲井和之、其田穣次、家上治雄、直野博光
"高精度比表面積細孔分布測定装置および2成分ガス吸着装置の開発"
Membrane, **27**, 337 (2002).

4) K. Nakai, J. Sonoda, H. Iegami, H. Naono
"High Precision Volumetric Gas Adsorption Apparatus"
Adsorption, **11**, 227-230 (2005).

5) M. Yoshida, Y. Senda, J. Sonoda, H. Naono, K. Nakai
"Adsorption Isotherm Measurement of N_2 from Extremely Low Relative

Pressure ($p/p_0 \sim 10^{-9}$) to Non-Porous and Microporous Carbon Materials"
Proceedings of the 9thInternational Conference on Fundamentals of Adsorption, pp. 20-25 (2007).

6) K. Nakai, J. Sonoda, M. Yoshida, M.Hakuman, H. Haono
"High resolution adsorption isotherms of N_2 and Ar for nonporous silicas and MFI zeolites"
Adsorption, **13**, 351-356 (2007).

7) K. Nakai, J. Sonoda, M. Yoshida, M. Hakuman, H. Naono
"High resolution argon adsorption isotherms for various zeolites"
Studies in Suface Science and Catalysis, **170A**, 831-836 (2007).

8) J. Sonoda, T. Kamegawa, Y. Kuwahara, K. Mori, H. Yamashita
"Preparation of Hydrophobically Modified Ti-containing Zeolite (TS-1) and Their Applications in the Liquid-phase Ammoximation of Cyclohexanone"
Bulletin of the Chemical Society of Japan (2010) (in press).

9) T. Kamegawa, J. Sonoda, K. Sugimura, K. Mori, H. Yamashita
"Degradation of Isobutanol Diluted in Water over Visible Light Sensitive Vanadium Doped TiO_2 Photocatalyst"
Journal of Alloys and Compounds, **486**, 685-688 (2009).

List of Other Publications

1) M. Yoshida, J. Sonoda, K. Nakai,

"Meso and Macro Porosity Measurement from Vapor Adsorption Isotherm"

Proceedings of the 7th International Symposium on the Characterization of Porous Solids, pp. 25-28 (2005).

2) K. Mori, T. Araki, S. Shironita, J. Sonoda, H. Yamashita

"Supported Pd and PdAu Nanoparticles on Ti-MCM-41 Prepared by a Photo-assisted Deposition Method as Efficient Catalysts for Direct Synthesis of H_2O_2 from H_2 and O_2"

Catalysis Letters, **131**, 337-343 (2009).